Mississippi State University
Scholars Junction

Theses and Dissertations | Theses and Dissertations

8-9-2008

Radio Frequency Evaluation of Oriented Strand Board

Xiaojian Liu

Follow this and additional works at: https://scholarsjunction.msstate.edu/td

Recommended Citation
Liu, Xiaojian, "Radio Frequency Evaluation of Oriented Strand Board" (2008). *Theses and Dissertations*. 3712.
https://scholarsjunction.msstate.edu/td/3712

This Dissertation - Open Access is brought to you for free and open access by the Theses and Dissertations at Scholars Junction. It has been accepted for inclusion in Theses and Dissertations by an authorized administrator of Scholars Junction. For more information, please contact scholcomm@msstate.libanswers.com.

www.manaraa.com

RADIO FREQUENCY EVALUATION OF

ORIENTED STRAND BOARD

By

Xiaojian Liu

A Dissertation
Submitted to the Faculty of
Mississippi State University
in Partial Fulfillment of the Requirements
for the Degree of Doctor of Philosophy
in Forest Products
in the Department of Forest Products

Mississippi State, Mississippi

June, 2008

www.manaraa.com

Copyright by

Xiaojian Liu

2008

www.manaraa.com

RADIO FREQUENCY EVALUATION OF

ORIENTED STRAND BOARD

By

Xiaojian Liu

Approved:

Jilei Zhang Associate Professor of Forest Products (Director of Dissertation)	Philip. H. Steele Professor of Forest Products (Committee Member)
J. Patrick Donohoe Professor of Electrical Engineering (Committee Member)	Moon G. Kim Professor of Forest Products (Committee Member)
Rubin Shmulsky Department Head and Coordinator Department of Forest Products	George M. Hopper Dean College of Forest Resources

www.manaraa.com

Name: Xiaojian Liu

Date of Degree: August 9, 2008

Institution: Mississippi State University

Major Field: Forest Products

Major Professor: Dr. Jilei Zhang

Title of Study: RADIO FREQUENCY EVALUATION OF ORIENTED STRAND BOARD

Pages in Study: 99

Candidate for Degree of Doctor of Philosophy

Oriented strandboard (OSB) is a wood-based composite product with the largest market share for residential and commercial construction. OSB composite products have introduced variability in their physical and mechanical properties due to their raw material and process variation. Reliable in-line non-destructive evaluation (NDE) devices are needed to rapidly determine OSB panel product quality during and after the manufacturing process.

Wood specific gravity (SG) and moisture content (MC) play an important role in the wood composite manufacturing process. A real-time after-press monitoring device for locating SG and MC variations can supply information needed to control and improve mat formation, hot press schedules, detect MC-related problems, reduce product variation, and perform final product quality inspection. No real-time non-contact NDE methods are available for simultaneous detection of MC and SG variation.

In this research, the radio frequency (RF) scanning technique was used to

www.manaraa.com

evaluate the MC and SG of OSB. The numerical simulation method assisted in developing RF sensors to nondestructively evaluate MC and SG of OSB composite specimens. MC and SG prediction models were derived based on RF testing results. The model behavior between relative humidity conditioned method and oven-drying conditioning method were compared.

The results indicated the RF scanning technique can be successfully used as a NDE tool to measure MC and SG of OSB panel products. Numerical simulation can help deciding RF sensor geometry successfully and accurately. The MC and SG of OSB can be predicted with the models developed with the procedure used in this study. The RF scanning results are not only influenced by material physical properties, but also influenced by their MC conditioning method, such as relative humidity conditioned method and oven-drying conditioning method.

www.manaraa.com

ACKNOWLEDGEMENTS

I wish to express my deep sense of gratitude and respect to my advisor Dr. Jilei Zhang giving me this opportunity to work in this project. I am indebted to him for his immense help, support and motivation at all times during my study and research.

I would like to express my sincere thanks to my committee members Dr. Philip H. Steele, Dr. Moon G. Kim and Dr. J. Patrick Donohoe for providing valuable guidance through out my study period.

I am thankful to other faculty and staff members at Department of Forest Products of Mississippi State University for their help and support.

Last but not the least, my heartfelt thanks goes to my wife and my family whose presence and support has been a constant source of inspiration for me to overcome all obstacles.

www.manaraa.com

TABLE OF CONTENTS

www.manaraa.com

www.manaraa.com

APPENDIX

www.manaraa.com

LIST OF TABLES

www.manaraa.com

www.manaraa.com

LIST OF FIGURES

www.manaraa.com

www.manaraa.com

CHAPTER I

INTRODUCTION

Wood-based composite products production volume has grown rapidly as new harvesting, processing and adhesives technologies have been developed. Substitution of composite products in housing construction has accelerated in recent years. An advantage of composite products is that their characteristics can be designed specifically to match the engineering needs of each industry. This provides an effective means of overcoming much of the variability imposed by solid wood products. However, composite products also have induced variability problems caused by wide differences in characteristics of the wood raw materials from which they are manufactured. Efficient and reliable measurement of the characteristics of the incoming wood raw material, of the in-process product during manufacture, and of the final composite panel product will insure a higher quality product.

Many of the current quality control procedures applied to monitor composite panel products are destructive tests following manufacture. Destructive tests are expensive and slow and problems discovered by such tests can allow a large volume of substandard products to be produced prior to detection and correction of the quality-degrading problem. Reliable in-line non-destructive testing (NDT) devices are needed

www.manaraa.com

to rapidly determine composite panel product quality during and after the manufacturing process.

Wood composites can be described as adhesive-bonded wood materials, usually produced under heat and pressure. Wood specific gravity (SG) and moisture content (MC) play an important role in the wood composite manufacturing process. They are the two of the critical variables that manufacturers are required to monitor, locate, and control in order to produce a product with consistent quality.

Physical, mechanical, and durability properties of wood composites are related to, and affected by, variations of SG and its distribution in panel horizontal (in-plane) and vertical (thickness) directions. MC variation of wood composites can produce internal defects such as blisters or blows during hot pressing. MC variation also slows the panel core temperature in reaching its optimum target. This can result in insufficient resin cure and reduced mechanical properties such as internal bond (IB) strength variance in the process. Strand layering during the forming process also causes for SG variation.

SG and MC variations express themselves in after-press panel properties. The product liabilities associated with undetected variations in these characteristics are non trivial. Therefore, a real-time after-press monitoring device for locating SG and MC variations can supply information needed to control and improve mat formation, hot press schedules, detect MC-related problems, reduce product variation, and perform final product quality inspection. No real-time non-contact NDE methods are available for simultaneous detection of MC and SG variation. Current after-press detection devices are limited to direct contact technology for the detection of blow defects.

www.manaraa.com

Radio frequency (RF) techniques have been successfully applied to estimate MC and SG of lumber by Steele and Cooper (2004). Steele and Cooper (2004) also claimed application of their patent to detection of MC and SG in composite products. However, no data supporting their claim was provided in the patent.

Oriented strandboard (OSB) is the composite product with largest market share for residential and commercial construction. In the North American structural sheathing market, the share of OSB increased from 4 percent in 1980 to approximately 58 percent in 2003 (Adair 2004). OSB production volume increased from 12.0 million cubic meters in 2003 to 12.6 million cubic meters in 2004; and for the first 5 months of 2005 OSB production was 2.1% higher compared to the same period in 2003 (Howard 2006).

This study describes using RF scanning technology to: develop sensors to nondestructively evaluate MC and SG of OSB composite specimens; and compare the influences of different MC conditioning method on RF responses of OSB specimens.

1.1 Objectives

The objectives of this research were to: (1) develop RF NDE dielectric sensors to detect MC and SG of OSB composite specimens; (2) derive regression equations to estimate SG and MC based on RF responses in terms of voltage attenuation and signal phase shift.

www.manaraa.com

CHAPTER II

LITERATURE REVIEW

Oriented strandboard (OSB) was developed in the latter half of the 20th century as a lower-cost structural panel than previously available structural panels. Higher-cost plywood has lost much of its previous market share to OSB. OSB panels are produced from oriented wood strands under high temperature and pressure with the help of waterproofed adhesives (Walker 2006). Due to the complexity of the manufacturing process, the physical and mechanical properties of OSB are influenced by many variables, such as raw materials properties, adhesive type, and process parameters. SG and MC play an important role in the OSB manufacturing process. They are two critical variables that manufacturers monitor, locate, and control in order to produce a product with consistent quality (Williamson 2002).

2.1 OSB manufacturing process

In the first step of OSB manufacture, small diameter logs are debarked and heated in soaking ponds, or are directly sent to stranders. Stranders cut strands from the logs to a width of 0.5" and ranging from 3" to 6" long. Strand thickness variability is controlled to about 0.03". (Walker 2006).

Green strands are then dried, typically in a rotating drum dryer. Strands are

www.manaraa.com

projected or blown to the surface of the drum and fall and tumble in a hot air stream for about 5 minutes. The inlet air temperature can be as high as 1500 °F, with the outlet temperature at approximately 240 °F. The final MC of strands leaving the dryer ranges from 2 to 5% (Walker 2006).

Dried strands are then transported to a blender where resin and wax are applied in an even distribution on strand surface. OSB panels are usually produced with PF resins as the adhesive. During the blending process, strand MC is increased to about 12% from water contained in the applied resin/wax adhesive compound (Walker 2006).

Adhesive-coated strands are next conveyed to a mat-forming machine. During mat forming, strands are aligned along the board length and others are aligned across the width before they are conveyed to the hot press. Mat density is measured continually during conveyor transport with a nucleonic device to ensure production of a uniform mat (Walker 2006).

After entering the hot press the mat is compressed and the resin cured to a structure-stable panel. Efficient production volume requires manufacture of multiple-opening presses. In these processes, sixteen 12-feet by 24-feet panels are compressed simultaneously at a temperature ranging from 350 to 400 °F. Hot pressing produces temperature gradients within the OSB panel in both the vertical direction from hot press platen surface to mat middle layer; and in the horizontal direction from mat center to the edge. These gradients create variations in density profiles and MC levels within the panel (Walker 2006).

Following hot pressing, OSB panels are ejected from the press and are sawn into 4-foot by 8-foot panels. These panels are then surface sanded and edge trimmed.

www.manaraa.com

Final adhesive cure occurs in cooling stacks into which the OSB panels are placed priors to packing and shipping (Walker 2006).

2.2 Moisture content variation

For wood products, MC is computed on a percentage oven-dry weight basis resulting in the potential for MC values greater than 100 percent. In live trees, the MC ranges from 50 to 200 percent. For most structural wood products MC value ranges from 4 to 20 percent. Wood product strength is increased by these moderate reductions in MC, but over drying can also result in reduced strength (USDA 1999).

As for all wood products, mechanical properties are significantly influenced by MC. When MC is below the fiber saturation point (FSP), normally 30%, wood mechanical properties increase with a decreasing MC (Gerhards 1982). Significant decrease of modulus of rupture (MOR), modulus of elasticity (MOE), and internal bond with increasing MC range from 10 to 15 percent were found in UF-bonded particleboard (Halligan and Schniewind 1974). Watkinson and van Gosliga (1990) discovered similar results for UF-bonded particleboard, medium density fiberboard (MDF), and hardboard. Wu and Suchsland (1997) noted a linear decrease in MOR and MOE with increased MC ranging from about 4.5 to 22 percent in PF-bonded OSB manufactured from both southern pine and aspen.

MC variations of the OSB mat can produce internal defects such as blisters or blows caused by production of steam at the high-MC location that ruptures the panel internally (USDA 1999).

www.manaraa.com

2.3 Panel horizontal density distribution

Wood product mass can be measured in terms of SG or density. Wood density is measured as weight per volume in lbs/ft^3. The wood MC for density purposes must be specified due to its influence on the weight component of the density computation. SG is introduced to reduce confusion from variations of MC and is defined as the oven-dry weight of the mass of dry wood to the equivalent volume of water.

In addition to MC variation, density variation significantly influences OSB panel quality. Density variation within the panel plane is defined as horizontal density distribution (HDD), and the density variation across panel thickness direction is termed vertical density distribution (VDD) (Suchsland 1962).

The HDD of panels immediately following hot pressing is inherited from the mat forming and hot pressing processes. Variation in mat thickness during forming will result in variance in panel horizontal density or HDD. When the mat is processed to constant thickness during hot pressing, some densified areas and some low density areas will be generated within the panel. Variance in strand thickness can also contribute to the HDD. Variation in HDD can lead to composite panels with low quality because differential spring back rate and thickness swelling between local areas will cause damaging panel stresses in panel (Suchsland 1962, 1973; Suchsland and Xu 1989, 1991). The European EN300 standard (2001) stipulates that composite HDD should be less than ±10% of the average panel density for structural OSB panel.

www.manaraa.com

2.4 Current wood composite density & MC detection methods

2.4.1 Non-electromagnetic density and MC detection methods

Application of sonic stress waves is a widely applied NDE technique for quality control for wood-based composite manufacture. Stress waves are generated by impacting or by a forced vibration. The impacting method is more desirable due to simplicity of stress wave generation. This method is utilized commercially by Metronground Technology to estimate plywood veneer strength for sorting purposes (Thomson 1981). Bulleit and Falk (1985) untilized stress wave technology to help power industry distinguishing strength-reducing decay from non-strength-reducing growth ring (ring shake). Researchers have also extensively used the sonic stress wave technology to evaluate the mechanical properties of lumber, wood composites, such as IB, MOE and MOR (Ross and Pellerin 1985).

Ultrasonic stress waves apply higher frequency waves compared to sonic waves allowing their concentration to a smaller area. Ultrasonic waves are used in both pass-through stress wave system and pulse-echo system. The former system has been used by researchers to investigate the mechanical properties of wood composites (Vun and Wu 2003). The latter method has been used to detect the voids and decay within wood composite panel (Wilcox 1988). There are no commercial systems based on ultrasonic stress wave technology applied to determine wood composite products moisture content or density.

www.manaraa.com

2.4.2 Dielectric properties of wood

Wood is a natural dielectric material with complex structure and composition (Torgovnikov 1993). The influence of alternating electric field on wood is significant, and this has led to commercial application of this concept for estimation of wood MC (Wagner 1996, Steele and Cooper 2004) and for knot and void detection in lumber (Steele and Kumar 1996).

When an electrical field is applied to wood, free electrons and ions present in conductive and semi-conductive molecules in cell walls, realign electrically. The molecules of water and cell wall substance polarize, with water polarizing to a negative charge and cell wall substance to a positive charge (Torgovnikov 1993).

The quantitative estimation of wood substance polarizability is defined as polarization intensity in Equation 1.

$$\mathbf{P} = (\varepsilon'-1)\,\varepsilon_0\mathbf{E} \qquad (1)$$

Where:

$\mathbf{P}$ = polarization intensity
$\mathbf{E}$ = electric field strength (V/m)
ε_0 = electric constant of a vacuum, $\varepsilon_0 = 8.854 \times 10^{-12}$ (F/m)
ε' = relative dielectric constant (real part)

The fundamental dielectric properties of materials are: permittivity (ε'), or relative dielectric constant, and dielectric loss tangent ($\tan\delta$). Permittivity defines the amount of polarization in a given material relative to that demonstrated in a vacuum. The loss tangent measures the energy absorbed by a material under the influence of an electrical field. The absorbed energy is converted to thermal energy as the

www.manaraa.com

electromagnetic wave propagates through the material. The (ε') and loss tangent (tanδ) of materials were first reported the earliest in the 1950's (Von Hippel 1954, James 1975).

To help determining the power dissipation in materials, a concept called complex dielectric constant (ε*) is introduced to the physics of dielectric materials. The response of wood materials to an applied electric field is different from that produced by the field in a vacuum. There are not only conduction currents (energy loss) but also displacement currents (energy storage) existing in the materials, which determine the active and reactive components of current energy. The complex permittivity is related to the loss tangent by Torgovnikov (1993)

$$\varepsilon^* = \varepsilon' - i\varepsilon'' = \varepsilon'(1 - i \tan\delta) \qquad (2)$$

where:

ε^* = complex dielectric constant
ε' = relative dielectric constant (real part)
ε'' = loss factor (imaginary part)
$\tan\delta$ = loss tangent, $\tan\delta = \varepsilon'' / \varepsilon'$
i = $\sqrt{-1}$

Descriptive equations of the interactions between an electromagnetic field and wood, contain ε' and tan δ and vary depending on the wood species, density, MC, and environmental temperature, as well as on the field frequency and its orientation in relation to the direction of the wood grain. The dielectric properties of wood-based materials are determined by the molecular structure of the different components of the material (Vermaas 1974). These properties refer to the specific interactions between dielectric materials and the alternating electromagnetic fields.

www.manaraa.com

2.5 Radio frequency scanning

Radio frequency (RF) signals or radio waves refer to that portion of the electromagnetic spectrum in which electromagnetic waves can be generated by alternating current fed to an antenna. The RF electromagnetic spectrum ranges from about 3 KHz to 300 GHz. Microwaves are a subset of RF, with a higher frequency range from 300 MHz to 3 GHz.

Torgovnikov (1993) demonstrated that wood dielectric constant (ε), and loss tangent (tgδ) values for radio frequencies from 20 to 1000 Hz, is strongly influenced by the wood moisture content and specific gravity.

Previous researchers have studied RF signals to estimate MC and SG of wood. Parker and Beall (1986) developed an adjacent capacitance electrode device to measure lumber moisture content. Sobue (2000) developed a device with adjacent capacitance electrodes to sense the moisture gradient in wood by employing what he termed the Electrode Scanning Moisture Analysis (ESMA) method. ESMA determines MC at various depths through wood thickness by manipulating the distance from 11 to 55 mm between adjacent electrodes on a single wood surface. Examination of the capacitance changes developed by manipulation of the electrode distance allowed computation of wood moisture gradient at various depths through wood thickness. This method allowed measurement of MC in wood up to 120 percent.

Jazayeri and Ahmet (2000) described an adjacent capacitance electrode method, similar to that of Sobue, for detecting transverse moisture gradients in timber. A multiple-planar-electrode arrangement was utilized to switch signal between pairs of electrodes at variant spacing to allow MC detection.

www.manaraa.com

Rice et al. (1992) developed a system to detect knots and voids in lumber utilizing non-contacting adjacent electrodes. This system detected the difference in dielectric properties between clear wood, knots and voids. Seven pairs of adjacent capacitors consistently detected knots and voids in lumber.

Steele and Kumar (1996) patented a device, the Detector for Heterogeneous Materials (DHM), for detecting specific gravity differences in scanned lumber by a radio frequency capacitance method using a 200 KHz AC signal. The DHM differs from the Parker and Beall device (1986), in that, opposed parallel plate detectors rather than adjacent electrodes are employed.

The dielectric response properties of knots, voids, and clear wood differ, and the DHM detects this difference by comparing voltage change within each piece of lumber. Recalibration for clear wood signal at any moisture content is performed for each piece of lumber based on a proprietary algorithm. For this reason, the bridge circuit component of the Parker and Beall device (1986) is not required. Conversion of amplified analog voltage to digital values and capture by data acquisition system is performed as for the Parker and Beall device (1986). To date, only detection of knots and voids has been described as being detected with the DHM (Steele and Kumar 1996).

Wolcott and Rials (1995) used the Eumetrics System III Micro-Dielectric Analyzer by imbedding miniature sensors in a formed mat, to monitor the in-situ cure of a particleboard panel produced with an isocyanate adhesive. They noticed the influence of MC changes to the dielectric responses during the process glue cure and the potential of dielectric scanning method using in real time detection of adhesive cure.

www.manaraa.com

This method employed embedded sensors in the wood panel during hot press. This method is, of course, is not possible for real-time dynamic scanning of boards.

Wang and Winistorfer (2003) developed a technology to nondestructively monitor the bonding development of particleboard during hot pressing using a dielectric system. The conductance of the panel was monitored in real time during hot pressing. They found a significant relationship between impedance signal level and panel strength. These researchers did not apply their method to estimate panel density.

Steele and Cooper (2004) described estimating MC and SG in their patent for the "Moisture and Density Detector" (MDD). This patent claims the potential of using the MDD for determining MC and SG of composite wood products. However, the patent data provided was only for lumber and with no information provided for a wood composite application.

None of the adjacent or opposed electrode devices for moisture or density detection reviewed above have been commercially used, with the exception of the DHM developed by Steele and Cooper (2004). This device, however, is utilized exclusively to detect density differences in solid wood products and identify knots and voids. A need exists for a sensing device to simultaneously measure MC and SG of wood composite products.

www.manaraa.com

2.6 Software simulation

Both wood and wood-based composites are complex heterogeneous materials possessing numerous characteristic variables that may influence an interacting RF field. Complete description of the interactions of these variables based on real-time experiments is made difficult due to the need for numerous samples, each with multiple varied characters. Finite element method (FEM) is a mathematical tool for solving engineering problems based on partial differential equations (PDE). This simulation method has been used to solve complex structural, thermodynamic engineering and electromagnetic problems that would be virtually impossible with real-time experiments (Reddy 1993).

The development of FEM element software capable of modeling electromagnetic phenomenon has offered researchers a powerful and rapid tool to characterize the interaction of electromagnetic waves with wood materials. Jin (2002) developed a 2D model to simulate the transverse electric (TE) wave transmitted through solid wood pieces. A more detailed FEM simulation on effects of microwave interaction with wood was developed by Hansson et al. (2006). They described that the effects of MC and SG to dielectric properties of wood, such as permittivity and conductivity, were significantly related. In their study, a microwave signal was transmitted through wood specimens by a pair of sending and receiving antenna. The transmitted and scattered waves were visualized with FEM software simulation. Wood permittivity and conductivity values, previously measured by the researchers, were used in the simulation. The simulation results were then verified with a medical

www.manaraa.com

computed tomography scanner, showing that the simulation accurately predicted microwave interaction with the wood.

2.7 Multiple linear regression

Multiple linear regression (MLR) is one of the most popular statistical modeling methods (Kutner et al. 2005). MLR models the relationship between two or more explanatory variables and a response variable by fitting a linear equation to observed data (Kutner et al. 2005). In this research, the MLR method was used to study the relationship between wood physical properties (moisture content and specific gravity) and wood dielectric properties (attenuation and phase shift).

The first step of MLR is variable normality checking. The normality checking of all predictors is necessary for satisfying the assumptions of regression analysis in practice (Mendenhall and Sincich 1989). The good performance of variable normality shows a good agreement with the linear regression assumption, which is that random error, ε, is normally distributed with mean 0 and variance σ^2 (Mendenhall and Sincich 1989).

The second step is data splitting. The ideal way of validating regression model is through collection of new data, while this is not always practical in the laboratory; because it is hard to duplicate all the influential factors to get the exactly the same data population at every time. The alternative method is equally splitting the experimental data set that is generated in the same time period when the data set is sufficiently large. These split data sets are the model-building data set and the validation data set. Normally the number of observations should be at least 6 to 10 times the number of

www.manaraa.com

variables in the pool of predictor variables. The model-building data set is used to develop the model. The validation data set is used to evaluate "the reasonableness and predictive ability" of the generated models (Kutner et al. 2005). The selection of the two data sets can be done randomly.

The third step of MLR is model-building that generates models by fitting regression equations using the model-building data set with the least squares method. Theoretically, when the controlled experiment is performed, there are unlimited combinations of predictors in terms of their orders. To avoid the cumbersome work of selecting too many orders of variables, dependent variables can be plotted against independent variables to learn their relationships. The maximum orders of predictors can be decided by looking at the previous scatted plot trend lines curvatures (Kutner et al. 2005). Among generated multiple candidate models, the ones with all regression coefficients passing the "t-test" with the p-values less than 0.05 will be saved for determination of the best fitted equation (Resch and Ecklund 1964). In the stage of model-building, the best fitted regression equation needs to be decided based on several model selection criteria. They are the coefficient of determination (R^2), the error sum of squares (SSE), and the mean square error (MSE) (Kutner et al. 2005).

The R^2 value is usually considered as a useful indicator of fitting goodness between the observational (real) values of the response Y_i, and the fitted (estimated) values $\hat{Y}_i$, while a large R^2 value does not necessarily confirm that the fitted model is a useful one. This is true, for example, when the observations are taken at a narrow interval and the predictions are located outside the region of observations. Even

www.manaraa.com

though the model R^2 may be large, MSE may still be too large for the explanation to be useful when high precision is required (Kutner et al. 2005).

The SSE indicates the sum of deviations between the observed value of the response Y_i, and the fitted value $\hat{Y}_i$ on the regression line. If all the Y_i values fall on the fitted regression line, the SSE equals to 0. The greater the variation Y_i around the regression line is, the higher the SSE is (Kutner et al. 2005). In another words, a regression line with a smaller SSE value is better than the one with a larger SSE value.

The MSE is an unbiased estimator of the square of standard deviation (σ^2). The predictive capability of fitted regression can be evaluated through studying the MSE. The lower the MSE is, the better fitting of the regression equation is (Kutner et al. 2005).

Stepwise regression is a popular model building method for MLR. This method automatically selects the most statistically significant variables from candidate explanatory variables with the help of statistical computer software (Kutner et al. 2005). In this research, we used the SAS (2006) program to perform the stepwise regression analysis.

There are three major stepwise regression approaches (1) forward selection; (2) backward elimination; and (3) mixed selection. The forward selection begins with the intercept term in the model. Each of the independent variables is plugged into the model, and the F-statistic is calculated to determine the variable's contribution to the model. The variables with the p-value of F statistic below a specified probability α (e.g., 0.15) will be kept in the model, otherwise will be removed. The process continues until all the remaining variables have been tested. The variable enters into

www.manaraa.com

the model will never be removed. The backward elimination selection includes all the variables in the model at the beginning. The p-value of F statistic of each variable will be calculated. The variable with p-value exceeding the specific probability α (e.g., 0.05) will be removed. The procedure continues until no remaining variables have F statistic p-values smaller than the α-to-remove. The variable being removed will never being added into the model again. The mixed selection is a combination of forward selection and backward elimination. After a variable is added into the model, all the variables in the model will be evaluated. Any variables with p-value exceed the specific p-value α-to-remove will be removed. Another variable will be added to the model after the previous one is removed and the procedure is repeated. The mixed selection ends only when all the variables remaining in the model are significant at the specific α, and all the variables removed from the model are not significant at the specific α (Young et al. 2008). In this research mixed selection stepwise regression were used to select the appropriate models.

The fourth step of MLR is model validation. Model validation refers to the process of evaluating the reasonableness of the regression coefficients, the usability of the regression function, and the ability to generalize inference of the regression model derived from model building data set (Kutner et al. 2005). In this step, the prediction sum of squares (PRESS) and the mean squared prediction error (MSPR) are used to check the validity of generated models from the model-building process.

The PRESS measures the deviation of observational response value, Y_i, from the fitted regression line. The PRESS criterion is obtained by first deleting the *i*th data point from the data set, then fitting a regression line to obtain the deviation between the

www.manaraa.com

Y_i and the regression line. By repeating the process through all of the variables for *i* times, the sum of squared deviations is calculated. The model with a smaller PRESS value indicates less prediction error. The PRESS value is always smaller than the SSE. This is because when the *i*th case is deleted in the fitting process; it will never be as good as when the *i*th case is included. A close approach of PRESS value to SSE value supports the validity of the regression model fitting. The comparison between PRESS and SSE is usually conducted in the regression model validation process (Kutner et al. 2005).

The MSPR uses the validation data set to evaluate the performance of the regression models generated from the model-building data set. A small difference between MSE and MSPR implies that the MSE of the model generated from model-building data set is a good indicator of the validity of the fitted regression model (Kutner et al. 2005).

Finally, to check the performance of the selected model, all experimental data including model-building and validation data sets will be plotted against predicted values from the selected regression model. A high correlation between predicted and actual experimental values in terms of higher R^2 of fitted straight lines is preferred. Also the slope of the fitted straight line close to 1 is desired (Jha et al. 2007).

The MLR method has been widely used in predictive modeling of product quality characteristics of forest products (Resch and Ecklund 1964, Hoover et al. 1992, Zhang et al. 1994, Muller et al. 2004, Palacios 2008). Also, it has been used in model development of non-destructive evaluation of material properties (Ross and Pellerin

www.manaraa.com

1985, Sweeting 1995, Brashaw et al. 1996, Olin and Meeker 1996, Simola and Pulkkinen 1998, Jha et al. 2007).

www.manaraa.com

CHAPTER III

MATERIALS AND METHODS

3.1 Approach

3.1.1 RF sensor development

The most effective RF scanning sensor geometries were tested with software simulation before experimental development. Software simulation was first employed to design the sensor shape. Following the determination of best sensor shape, the optimum sensor size relative to conductor width was simulated in terms of the highest electric field strength produced. Finally, optimum sensor spacing was decided to minimize interaction among multiple sensors.

3.1.2 Model development

OSB specimens of various density levels were fabricated. These specimens were then divided into two groups and subjected to two different MC conditioning methods.. One OSB group was conditioned to desired MC levels with the relative humidity conditioning method. The other OSB group was kept in 12% relative humidity chamber to reach about 12% MC, and then oven-dried to different MC levels. After conditioning to targeted MC levels, responses of the OSB specimens to the RF field in terms of voltage attenuation and phase shift were evaluated with the RF scanning apparatus. The MLR method was applied to develop and validate regression

www.manaraa.com

models to establish functional relationships between estimated variable MC and estimator variables attenuation (Att) and phase shift (Phase), and also between estimated variable SG and estimator variables Att and Phase.

3.2 Experimental Design

3.2.1 Sensor shape study

Two sizes of squared sensors (4" and 5" in width) and two sizes of rounded sensors (4" and 5" in diameter) were simulated to obtain information on influence of sensor shape. One simulation for each of the sensor sizes was conducted on one simulated OSB sample size. The simulated OSB sample size was 8" wide by 8" deep by 0.5" thick.

3.2.2 Sensor size study

3.2.2.1 Software simulation method

Twenty-one simulation models of combinations of 3 sizes (6", 4" and 3" in width, 0.5" in thickness) of square sensors and 7 sizes (8", 7", 6", 5", 4", 3" and 2", 0.5" in thickness) of squared wood samples were created to study size effects on the electric field strength. The influence of sensor size on the electric field strength (E) distribution was studied.

www.manaraa.com

3.2.2.2 Experimental method

Three sizes (6", 4" and 3" in width, 0.5" in thickness) of squared sensors and 7 sizes (8", 7", 6", 5", 4", 3" and 2", 0.5" in thickness) of squared OSB samples were investigated. All the signal sending and receiving sensors were the same size for each of sensor pairs. Two density levels, 35 lb/ft^3 and 50 lb/ft^3, of OSB specimens with 8" by 8" in width with 1 replication were initially RF tested. Specimens were edge cut by removing 0.5" on each side to obtain a 1" width decrease was achieved before each RF test.

3.2.3 Sensor spacing study

Eleven levels of sensor separation (0, 0.5", 1", 1.5, 2", 2.5", 3", 3.5", 4", 4.5", and 5") were investigated. A square OSB panel (24"x 24" x 0.5" in size, 40 lb/ft^3 in density) was used in this part of study.

3.2.4 Relative humidity conditioning

An experiment with six SG levels (0.50, 0.57, 0.59, 0.66, 0.69 and 0.74) and seven MC levels (2.5%, 3.5%, 4.5%, 6.9%, 8.5%, 10.1% and 12%) with 2 replications for each of 42 combinations was performed. Therefore, a total of 84 samples were measured individually for their RF responses in terms of voltage attenuation (Att) and signal phase shift (Phase) to derive regression equations for estimation of OSB SG and MC using the RF responses. From the 2 replications of each of the 42 combinations, one was randomly selected as the model-building data set with the remaining specimen as the validation data set. Specimen sizes measured 5" wide by 5" deep by 0.5" thick.

www.manaraa.com

The width and depth of specimens were determined through RF field range simulation and experiment for the various RF sensor shapes and sizes.

3.2.5 Oven-drying conditioning

To determine influence of specimen response to oven-drying reduction of moisture content specimens with 6 SG levels (0.46, 0.53, 0.56, 0.58, 0.60, and 0.68) and 7 MC levels (2.5%, 3.5%, 4.5%, 6.9%, 8.5%, 10.1% and 12%) with 2 replications were conducted. Therefore, a total of 246 combinations were generated. In each combination, one of the 2 replications was randomly selected as the model-building data set with the remaining specimen entering the validation data set.

3.3 RF testing apparatus

The elements of the apparatus for transmitting the RF field through the OSB specimens are shown in Figure 3.1. Electrodes of copper plate comprised the RF capacitor with a sending and a receiving electrode. The RF signal was generated with an HP™ 8647A signal generator and amplified by a 10-Watt ENI™ 441LA signal amplifier. The amplified signal was applied to the transmitting electrode producing an electric field sensed by the receiving electrode. The amplified signal applied to the sending electrode was simultaneously input to one channel of Tektronix™ TDS714L digital storage oscilloscope as reference. The signal amplitude in volts and frequency in degrees were displayed on the oscilloscope. The signal received by the receiving electrode was input to the second channel of the oscilloscope. The phase value difference in degrees between the signal input to the sending electrode and that at the receiving electrode was measured automatically by the oscilloscope. All connecting

www.manaraa.com

cables in this apparatus have the same characteristic impedance value of 50 Ohms matching the output and input impedance of all devices in this application.

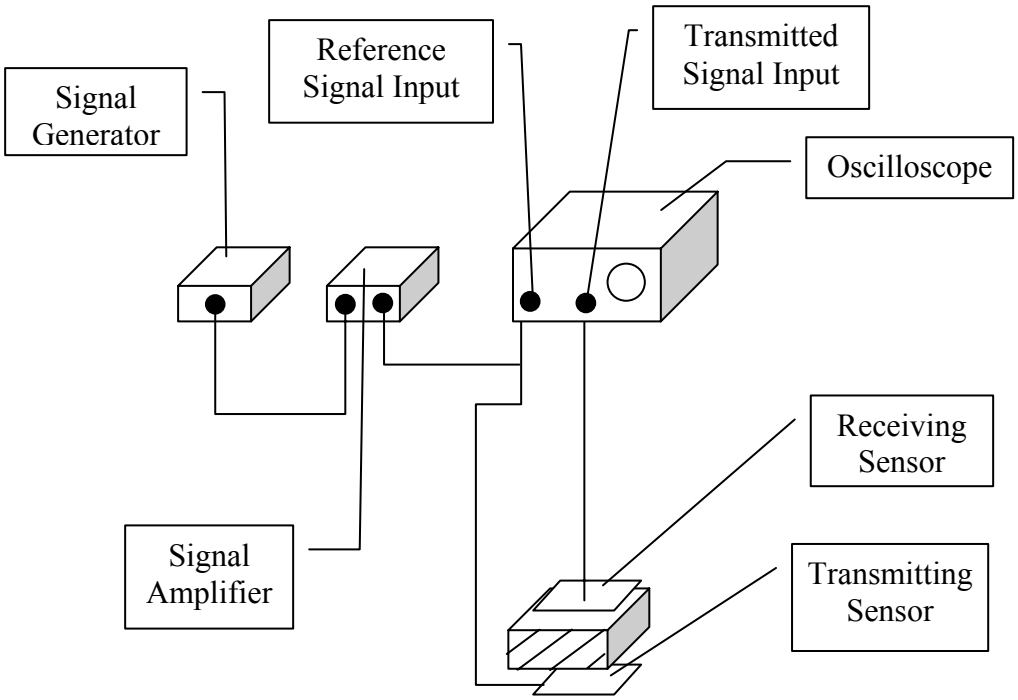

Figure 3.1 Diagram of single pair sensors RF scanning apparatus.

The phase shift was expressed as the difference in degrees between the phase of the transmitted and the received signal (Equation 3-1). The signal voltage attenuation in decibels was measured with the voltage logarithm of the ratio of the signal voltage on the transmitting sensor, $V_{transmitting}$, to the signal voltage on receiving sensor, $V_{receiving}$, (Equation 3-2).

$$\text{Phase shift} = \text{Phase}_{\text{transmitting}} - \text{Phase}_{\text{received}} \quad (3\text{-}1)$$

$$\text{Attenuation} = 20 * \log\left(\frac{V_{transmitting}}{V_{receiving}}\right) \quad (3\text{-}2)$$

www.manaraa.com

The actual setup was shown in Figure 3.2. The scanning table was custom made. A piece of OSB panel (32”x 32” x 0.75” in size) was cut as the base board of the scanning table. Four adjustable legs were fitted at the four corners of the base board. Four supporting wheels were fixed on an OSB strip (22”x2.75”x0.5” in size) as a support wheel group. Each supporting wheel group was installed on the base board with three 5” threaded bolts. A total of 3 groups of supporting wheels were installed on the base board. Two pieces of sensor supporting strips (28” x 2.5” x 0.25” in size) were made from plexiglass. A slot of 24” by 0.5” was cut in the center of each supporting strip to enable changing sensor spacing easily. The two supporting strips were installed on the base board with two 9” threaded bolts. All the heights or distances between supporting wheels groups and sensor supporting strips can be easily adjusted.

www.manaraa.com

Figure 3.2. The actual RF scanning apparatus.

www.manaraa.com

3.4 Procedure

The purpose of sensor shape, size and spacing study was to investigate their effects on effective RF field; therefore the optimum RF sensor shape, size, and spacing between sensors can be determined. Two sensor shapes, square and round were considered first. Considering in multiple sensors application, the cover area of electric field generated from squared or rounded shapes are different. The sensor shape and spacing between sensors needs to be determined to effectively cover all the board area between the sensors.

The COMSOL multi-physics finite element modeling software was chosen as the simulation tool to visualize the sensor shape and size effects on the distribution and strength of the electric field. In addition to simulation, an experiment was performed to verify the simulation results.

3.4.1 Sensor shape, size and spacing study

3.4.1.1 Software simulation setup

Effects of various sensor shapes and sizes on the distribution of the electric field through tested specimens were investigated with the COMSOL Multiphysics finite element modeling (FEM) software. The 3D geometries of the testing apparatus were developed in accordance to the actual dimensions. Figure 3.3 illustrates one of the 3D models showing the RF sensor and specimen geometries. The signal sending sensor was located above the tested specimen and the receiving sensor was located below specimen. Both sending and receiving sensors were identical in size and shape. A

www.manaraa.com

square, 8” by 8” wood specimen with 0.5” thickness was placed between the two sensors. The square sensor measured 4” on each side. The gap between the specimen and the sensor was 0.1”.

The sensor was made from a single sided printed circuit board with 0.06” thick substrate. Both sending and receiving sensors were connected to the coaxial cables with an inner conductor (diameter = 0.035”) and an outer conductor (diameter = 0.116”).

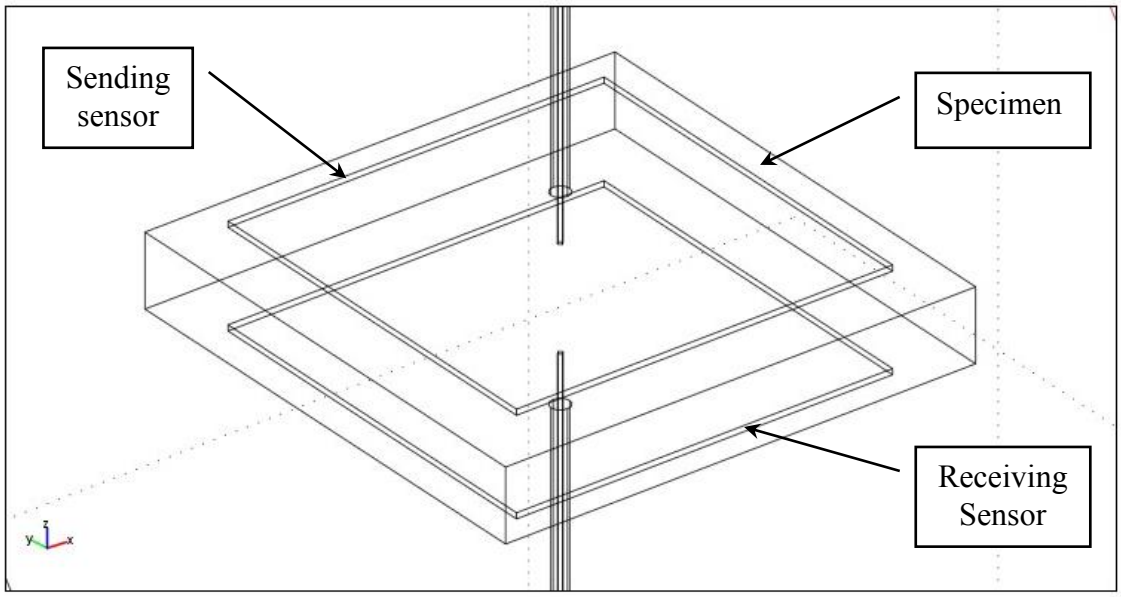

Figure 3.3. The geometry of a 3D simulation model.

Boundary conditions and domain parameters were specified in the model to define the material properties of RF devices and the specimen, and to quantify the RF signal magnitude and directions applied on the sensors. Because there was no OSB dielectric property available such as relative permittivity and conductivity, dielectric

www.manaraa.com

property data of solid wood from reviewed literature at similar MC and SG levels were used in the simulation process.

The dielectric properties of longleaf pine measured at MC=10%, SG=0.59, and at 100 KHz signal frequency were obtained from Wood Handbook (USDA 1999) and from the research performed by James (1988). The specified relative permittivity (ε_r) was 4.4, and the conductivity (σ) was 7.576 x10^{-10} s/m. These dielectric properties were input to the simulation model by setting up the sub-domain parameters of the wood specimen. An AC input voltage of 80 volts was specified as the boundary condition setting for the input source. The input sensor and the inner connector of the coaxial cable were specified to be 80 volts of electric potential, and the outer connector of coaxial cables were grounded (0 volts). The simulation program optimized the solver parameters to save calculation time, and the meshing and solving procedures were automatically conducted. Final results of the electric field were displayed with a color spectrum indicating the strength and direction.

3.4.1.2 Experimental method

3.4.1.2.1 Sensor size study

The influence of square sensors was simulated based on both voltage attenuation and required scanning resolution. Because the received RF signal strength in voltage is proportional to the area of the sensor, the larger the sensor, the higher the received signal voltage will be. A higher voltage is always desirable for a received signal because it provides more stable readings and also overcomes most of the background noise. However, larger sensor area reduces the scanning resolution. The

www.manaraa.com

sensor size study was performed by measuring the signal attenuation accompanying the change in sensor sizes.

The RF scanning device scanned the specimens of two densities with each of the three pairs sensor plates. For each of the three sensor sizes the signal attenuation for each specimen and the distance between sensor and specimen edges was recorded. The initial size of OSB specimen was 8", therefore the distance between the sensor edge to the specimen edge were 1", 2" and 2.5" for 6", 4" and 3" size sensors, respectively. After recording the data, the two OSB specimens had 0.5" at each edge removed with a band saw. For each reduction in OSB specimen size the RF testing was repeated. OSB specimen size was reduced by 1" in dimension, 6 times until the size of the OSB specimens reached 2" by 2". The applied RF signal was AC, 80 volts, and the frequency was 250 KHz.

3.4.1.2.2 Sensor spacing study

Two pairs of sensors with the same selected optimum size were tested in the sensor spacing study. One sensor pair was fixed on a supporting rack while the second sensor pair was moved to change the edge distances (spacing) from the fixed sensor. The sensor spacing study was performed on an OSB panel conditioned in the 12% EMC chamber for 2 months. The panel density was 42lb/ft^3. The AC signal voltage was 80 volts and the frequency was 250 KHz. The signal generated from the signal generator was split and sent to the sending plates. The Received signal was transmitted to the oscilloscope measuring the Att and the Phase.

www.manaraa.com

For each spacing level, Att values of both sensors pairs were recorded. Then the Att of the fixed sensor was measured again once the moving sensor was removed. The Att values of the fixed sensor, with and without, the second sensor present were compared. The purpose was to determine the spacing at which the influence from one sensor to the other could be neglected.

3.4.2 OSB raw materials

Southern yellow pine OSB flakes (3.4" x 0.4" x 0.07") were obtained from Norboard Mississippi Inc., Guntown, Mississippi. The strands were selected from furnish exiting the drying process. Strands were kept in sealed buckets until making boards. Measured strand MC was 3-4%. Phenol-formaldehyde (PF) resins and wax were obtained from Georgia-Pacific Resins, Inc. Louisville, Mississippi. Two PF resin solid contents, 60% and 50%, were used for core layer and surface layer, respectively. The emulsion-type solid content of the wax was 50%.

3.4.3 OSB panel fabrication

OSB panels of 24"s wide by 24" long were fabricated with 6 target densities (35, 40, 41, 42, 45 and 50 lb/ft^3), which corresponding to the 6 SG levels. Each density level had 2 replications. Weight percentages of strands, resin, and wax for each target board are given in Appendix A.

OSB strands were dried in a drum dryer (Figure 3.4) to reach a MC below 4% based on the wood oven-dried weight. The flake MC was constantly checked during drying with a moisture balance. After the strands MC reached 4%, they were put into a rotary blender. The diameter of the rotary blender was 1.8 m in diameter and 1.2 m in

www.manaraa.com

depth. The rotary speed was 22 rpm. Wax and resin were injected into the blender by means of a peristaltic pump. An air-compressed spray nozzle (Spraying System Co.) sprayed the emulsion-type wax onto the strands. A spinning-disk type atomizer (Coil Model EL-2, 1047 rad/s (10,000 rpm)) sprayed resin onto the strands following the wax application. The total blending time was approximately 15 min.

Core and surface layer flakes were blended with wax and resin separately in terms of their different solid contents. The layer constructions of top, core and bottom layer were 30%, 40% and 30% of total dry furnish weight respectively. The flakes were hand formed in random orientations with a 30" by 30" wooden forming box.

The formed mats were then hot-pressed in a Dieffenbacher hot-press. The platen temperature was 210 ºC (410 ºF), and the pressing time was 4 minutes. Following hot pressing the OSB panels were air cooled to room temperature and edges were trimmed to 24" by 24" dimension specimen. OSB specimens were stored in a 12 percent EMC conditioning room for two months.

3.4.4 Specimen preparation

Two randomly-selected groups of OSB specimens were prepared for the experiment. Group I of 84 specimens were conditioned using the relative humidity conditioning method. Group II of 24 specimens were conditioned using the oven-drying method.

www.manaraa.com

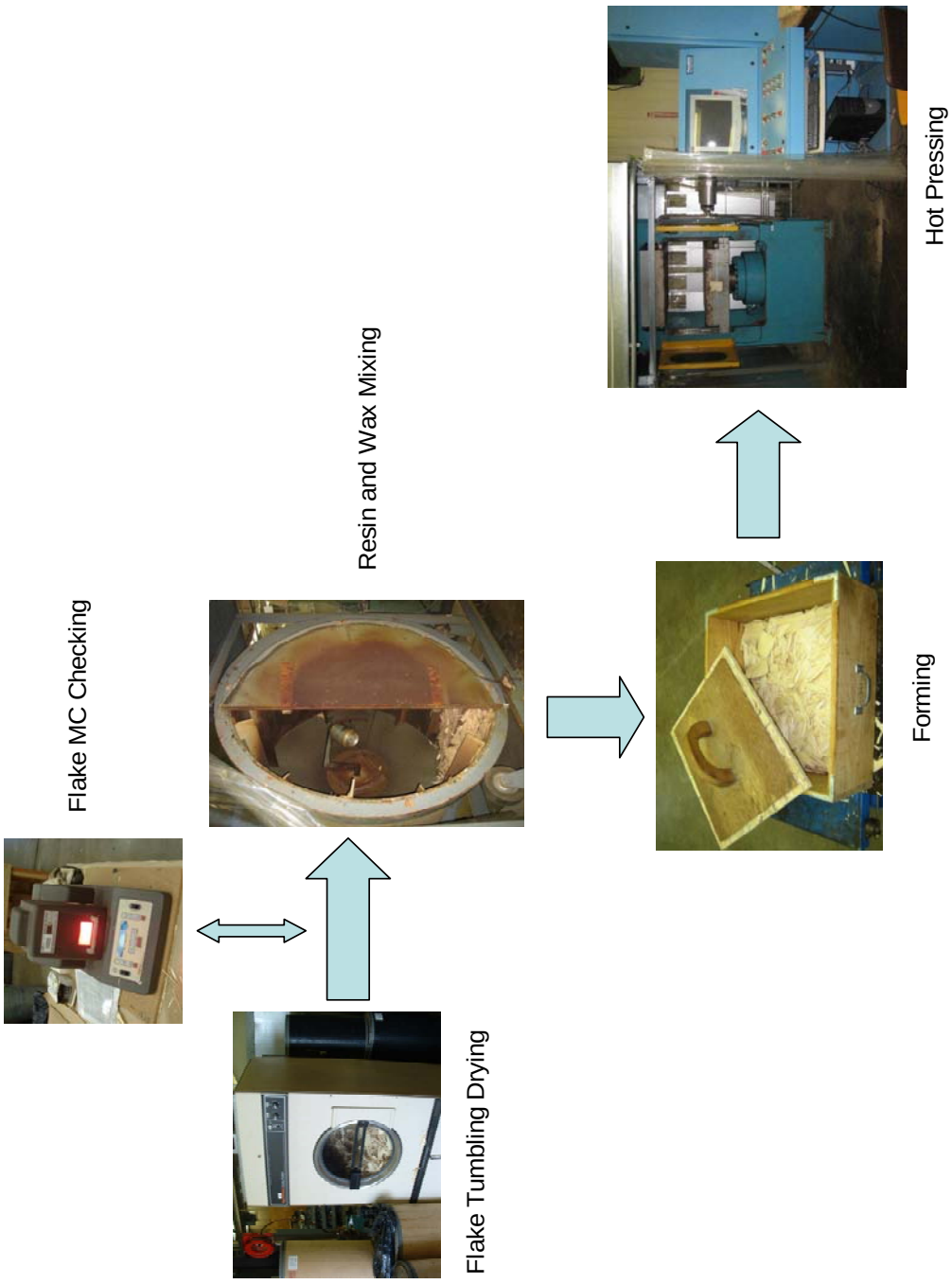

Figure 3.4. The diagram of OSB fabrication process.

www.manaraa.com

3.4.4.1 Relative humidity conditioning

Equilibrium moisture content (EMC) of wood is defined as the MC at which wood neither gains nor loses moisture when stored in an environment with stable temperature and relative humidity (USDA 1999). OSB specimens were conditioned to 7 levels of MC conditions with saturated salt solutions in sealed tanks at constant temperature of 20 °C according to ASTM E104-02 (2002) and ASTM D4933-99 (2004). Greenspan (1977) reviewed the method of controlling relative humidity in a sealed tank with several saturated inorganic salt solutions. No data is available for the relation between the EMC of OSB with relative humidity conditions. EMC data of wood-based composites products listed in Table 3.1 were used as reference (Greenspan1977, ASTM 2004).

Table 3.1 EMC data for composite wood products (Greenspan1977, ASTM 2004)

Saturated salt solutions	Relative humidity (%)	EMC (%)
Zinc bromide ($ZnBr_2$)	7.94 ± 0.49	1.5-2
Lithium chloride (LiCl)	11.31 ± 0.31	2-3
Potassium acetate (CH_3COOK)	23.11 ± 0.25	2-6
Magnesium chloride ($MgCl_2$)	33.07 ± 0.18	5-7
Potassium carbonate (K_2CO_3)	43.16 ± 0.33	5-8
Magnesium nitrate ($Mg(NO_3)_2$)	54.38 ± 0.23	7-9
Sodium nitrite $NaNO_2$	75.36 ± 0.35	9-11

www.manaraa.com

The 7 targeted MC levels of OSB specimens were obtained by conditioning the 84 OSB specimens in 7 relative humidity conditioned chambers. Each of the 24" by 24" OSB panels were previously stored in the 12 % EMC conditioning room for two months. Prior to storage in the smaller salt-conditioned relative humidity chambers the 24" by 24" specimens were cut into three 6" by 8" samples.

Figure 3.5 shows the actual setup of the seven salt conditioned relative humidity chambers. Seven commercially available 10 gallon (20" x 12" x 10.5") aquarium fish tanks were obtained and a 20" by 10.5" lid of 1/10" thickness was fitted. Dow Corning high vacuum grease was applied around the edges between the fish tank and the lid to seal the tank. A fan (3" x 3" square, RadioShack) was installed on the lid and inside the tank to provide good air circulation and expedite establishment of EMC in the OSB specimens. A glass baking tray (12"x 8" x 2") was held the saturated inorganic salt in the bottom of the tank. A plastic rack supported the OSB specimens above the salt solution, and also separated the specimens to insure good air circulation. To insure over-saturated status of the salt solution, the presence of salt crystals was monitored every two days during the conditioning process. Adequate amounts of inorganic salt were added when the redundant salt crystal was found dissolved.

www.manaraa.com

Figure 3.5. Relative humidity conditioning tank using saturate salt solution.

www.manaraa.com

3.4.4.2 *Oven-drying conditioning method*

The 24 8"by 6"specimens that had MC manipulated by oven drying were initially conditioned in the 12% EMC chamber. They were then gradually oven-dried (103 ºC) to 0% MC. Following over drying the specimens were air-cooled to room temperature after being taken out of the oven to prevent the temperature influence on RF scanning results.

3.5 Regression analysis

The MLR method was applied to analyze the RF testing data and develop the prediction models. Tests for normality of the Att and Phase independent variables were performed. The model-building data set was fitted to several linear models by the least squares method, and then the best fitted linear model was selected with stepwise regression method (Mendenhall and Sincich 1989). Finally, the best-fitted regression models were evaluated for prediction performance by comparing the predicted and the measured MC and SG.

Statistical analyses were performed with statistical software package (SAS 2006). Unless otherwise specified, all statistical analyses in this study were performed at a significance level (alpha) of 0.05.

www.manaraa.com

CHAPTER IV

RESULTS AND DISCUSSION

4.1 Sensor shape and size study

4.1.1 Simulation method

4.1.1.1 Sensor shape study

Figure 4.1 shows the patterns of electric field strength (E, V/m), located at wood specimen middle cross section in the thickness direction. The absolute value of E ranges from 10.3 V/m at the lowest value to the 1934.3 V/m at the highest value. Numbers indicate the color spectrum obtained in the simulation images. The number 1 indicates electric field strength of 1400 V/m and above; the number 2 indicates electric field strength ranges from 600 V/m to 1400 V/m; and the number 3 indicates electric field strength below 600 V/m. The higher the electric field strength is, the stronger the electric field. The numerals designating the simulation false color spectrum clearly show the E patterns always follow the shape of sensor which generates the electric field. Therefore, sensors generate the same shape electric field in specimen cross section. In multiple sensor setups, the square electric fields can be aligned side by side to eliminate uncovered areas that always exist between electrical fields from sensors of round shape. Therefore square shape sensors will always provide superior coverage of panel area.

www.manaraa.com

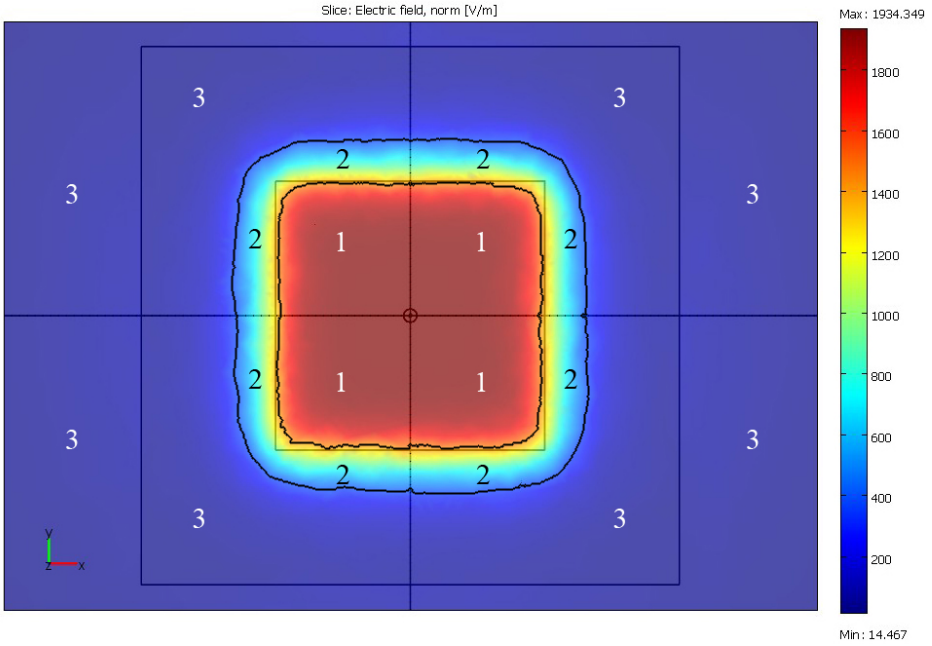

(a)

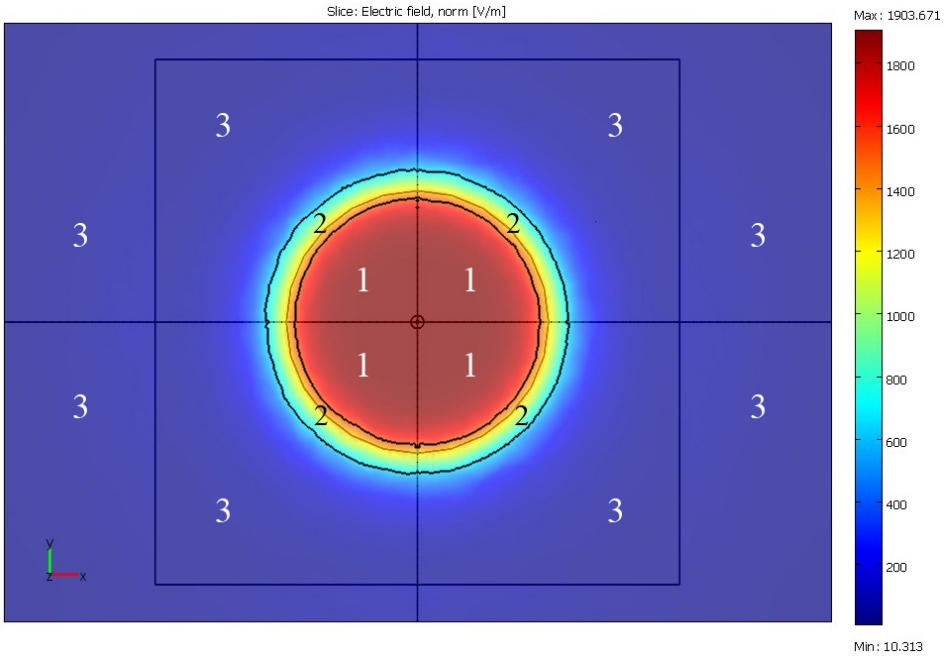

(b)

Figure 4.1. Electric field plots of (a) square shaped sensor, and (b) round shaped sensor; electric field strength, region (1) 1400 V/m and above; (2) 600 – 1400 V/m; and (3) 0 – 600 V/m.

www.manaraa.com

4.1.1.2 Sensor size study

Plots of a, b, and c of Figure 4.2 show the simulation results of E for sensor sizes, 6", 4" and 3", respectively. The specimen size measured 7" square. The numeral 1 indicating false red color, representing a strong electric field in the specimen cross section, is always confined within the sensor area. The magnitude of E decreases quickly outside the sensor boundary. For all three sensor sizes, the color changes from light blue to dark blue (numeral 3) at a distance of about 0.5" from the sensor edges, which indicates that E sharply declines from 600 V/m to below 100 V/m at this short distance from sensor edge. Therefore, the strong electric field is always within the area about 1" larger in width than the sensor size regardless of sensor dimension.

Figure 4.3 shows similar results but from a different approach. The sensor size was fixed at 4" and the specimen width reduced from 7" to 2". The strong electric field remains about 1" bigger in width than the 4" sensor size. Therefore, the effective electric field size is about 5" wide by 5" deep for 4" wide sensors, no matter how large the specimen size.

All three sizes, 6", 4" and 3" sensors have the effective electric field sizes of about 1" larger than their sensor sizes, respectively. The largest sensor size (6") will, of course, provide lowest resolution and smallest sensor size (3"), the highest. However, based on the experimental trials, the larger the sensor plate area, the higher voltage the received signal.. Therefore, the 4" size sensor was selected for RF testing, yielding an effective electric field size of 5" wide by 5" deep.

www.manaraa.com

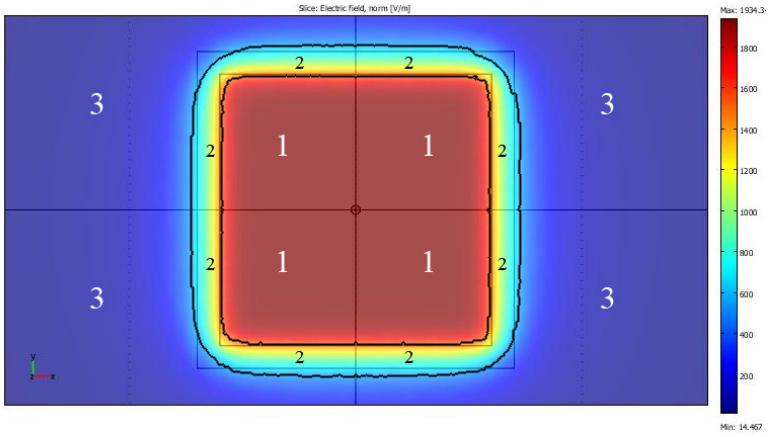

(a)

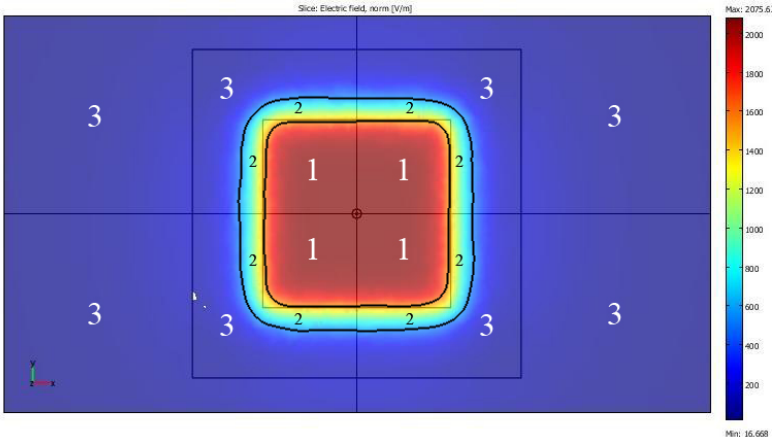

(b)

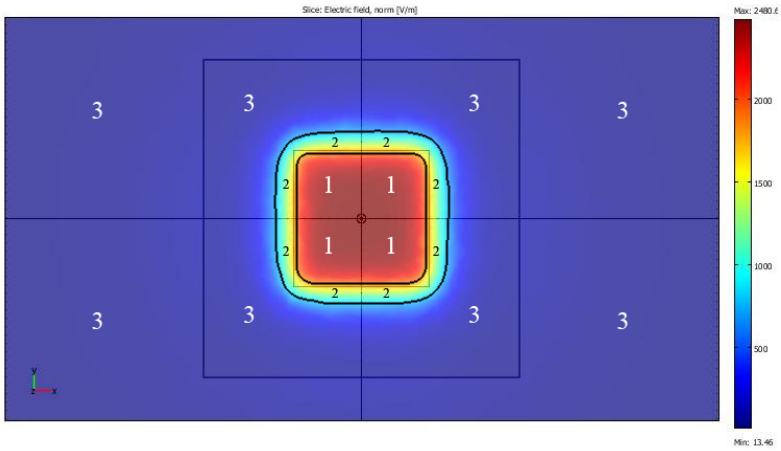

(c)

Figure 4.2. Electric field strength plots of a specimen with 7” in width, and sensors with (a) 6”, (b) 4” and (c) 3”in width, respectively; electric field strength, region (1) 1400 V/m and above; (2) 600 – 1400 V/m; and (3) 0 – 600 V/m.

www.manaraa.com

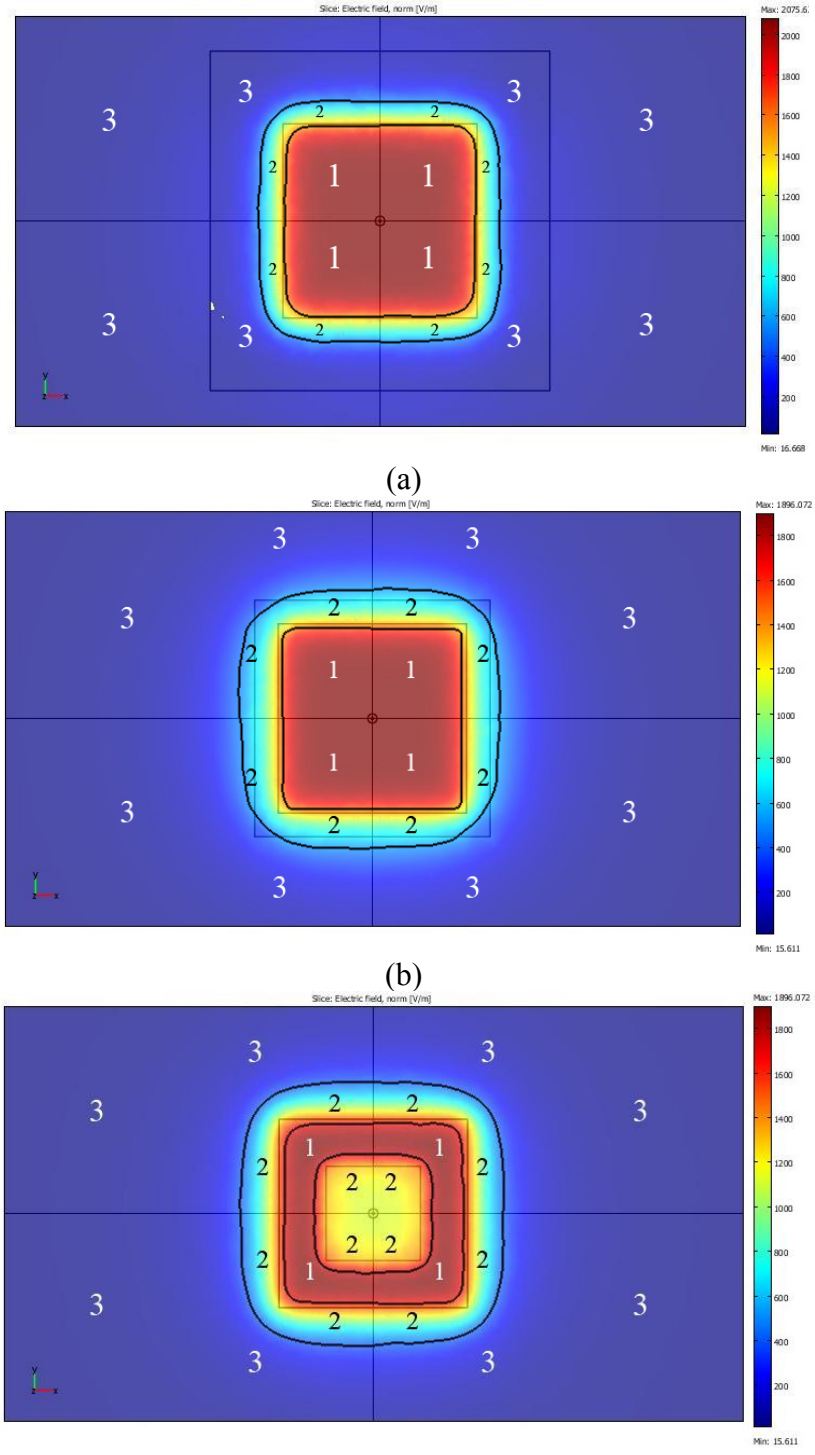

Figure 4.3. Electric field strength plots of sensors with 4” in width, and specimens with (a) 7”, (b) 5” and (c) 2”in width; electric field strength, region (1) 1400 V/m and above; 92) 600 – 1400 V/m; and (3) 0 – 600 V/m.

www.manaraa.com

4.1.2 Experimental method

4.1.2.1 Sensor size study

The experimental results of signal attenuation versus distance between sensor edge and specimen edge are summarized in Figure 4.4. In general, there was no significant change in attenuation when the distance between sensor edge and specimen edge was greater than 1". But, the signal attenuation increased slightly as the distance decreased from 0.5" to 0".

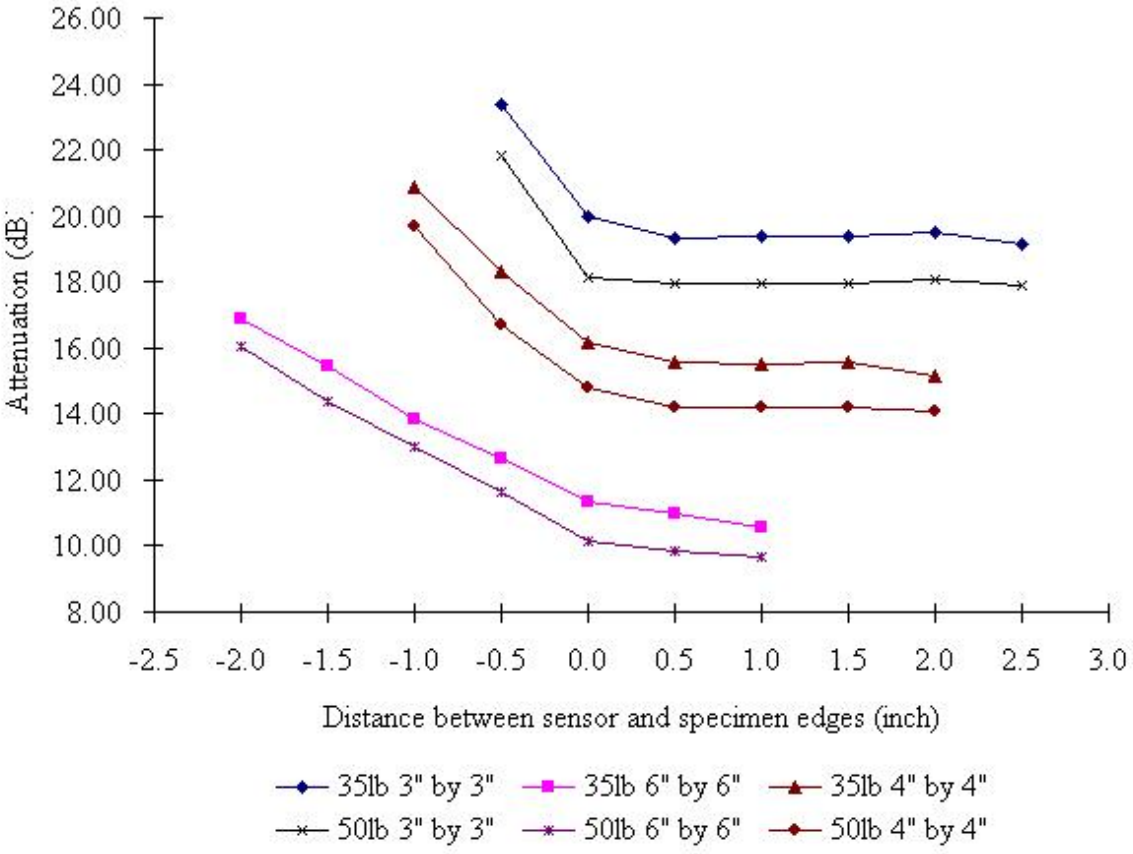

Figure 4.4. Attenuation versus distance between sensor and specimen edge.

www.manaraa.com

The signal attenuation decreased significantly when the distance was below 0", which indicated specimen size was smaller than sensor size. These results indicated that the signal attenuation level is not significantly influenced by material outside area which was 1" larger than sensor size. The threshold size difference was 1". Therefore it was concluded that the effective scanning areas for the 3", 4" and 6" sensors are 4" by 4", 5" by 5" and 7" by 7", respectively.

4.1.2.2 Sensor spacing study

Figure 4.5 shows the attenuation versus the sensor spacing. When the spacing between two sensor edges was 0, the attenuation of sensor 1 was 18 dB, which was about 0.5 dB higher than the one of sensor 1 with sensor 2 removed. This indicated that sensor 2 influenced the signal received by sensor 1 when the spacing was 0. As the spacing increased from 0 to 1", the sensor 1 attenuation reading approached the same value obtained in the absence of sensor 2.

www.manaraa.com

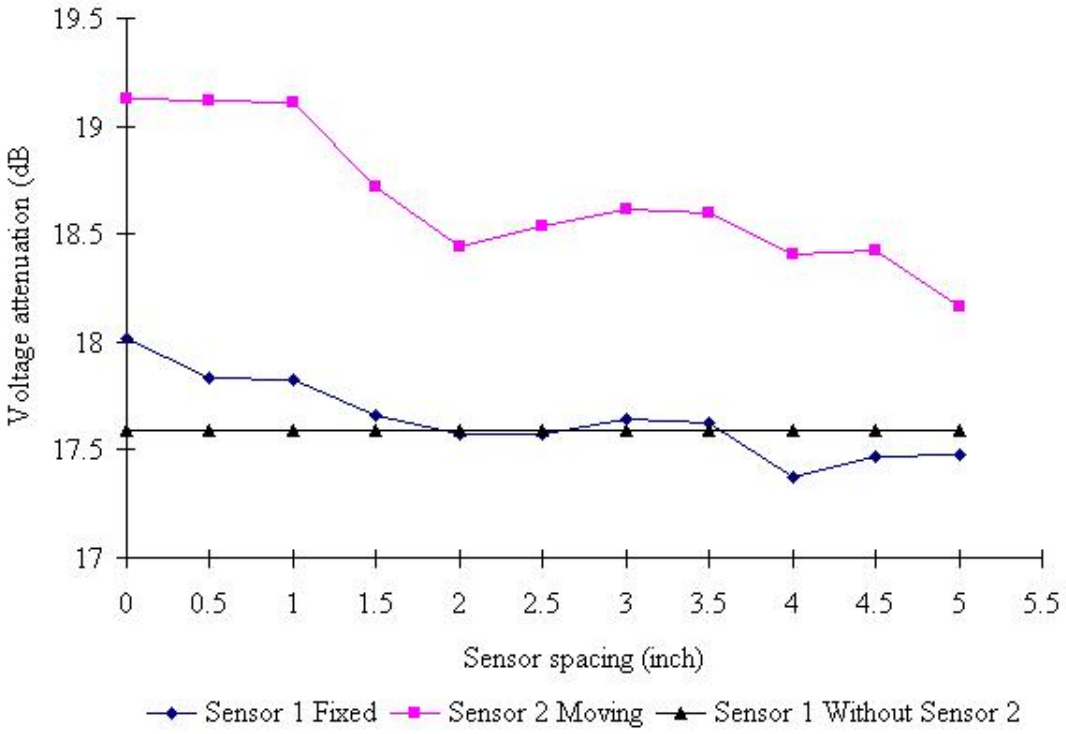

Figure 4.5. Voltage attenuation by sensor spacing from RF apparatus results.

This result indicated the influence of sensor 2 on sensor 1 decreased as the spacing increased. The attenuation of sensor 1 was equal to that obtained in the absence of sensor 2 as the spacing approached to 1.5". This indicates the influence of sensor 2 on attenuation of sensor 1 is absent when the between-sensor distance is greater than 1". Therefore, for 4" size sensors, when the spacing between two sensors is over 1", multiple RF sensors can be treated as stand-alone sensors.

It can be concluded that based on simulation and experimental results, the shape of effective electric field for RF scanning sensor was the same as the sensor. For this reason square sensors of 4" width were selected for RF testing as the best shape and size. Square sensors of 4" width have a square shape effective electric field

www.manaraa.com

measured 5” in width. In case of the multiple sensors RF testing, the spacing between sensor pairs should be at least 1”.

4.2 Regression analysis

4.2.1 Relative humidity conditioning method

4.2.1.1 Model development

4.2.1.1.1 Data normality testing

The UNIVARIATE procedure was used to conduct the data normality test on both model-building and validation data sets. Results (Appendix B.1.1 and B.1.2) of the Shapiro-Wilk test (Kuter et al. 2005) indicated that the normality assumption for each variable was confirmed with a p-value greater than 0.05. The normality probability plot for each of two predictors, Att and Phase, of both model building and validation data sets was a straight line that indicated the variable was normally distributed.

4.2.1.1.2 Model selection

Figures 4.6 and Figure 4.7 show the scatter plot of MC and SG versus predictor variables (phase and attenuation) of model-building samples, respectively. Attenuation had a clear linear relationship with both MC and SG. There was a slightly curved relationship between phase and MC. However, no clear trend can be identified between phase and SG.

www.manaraa.com

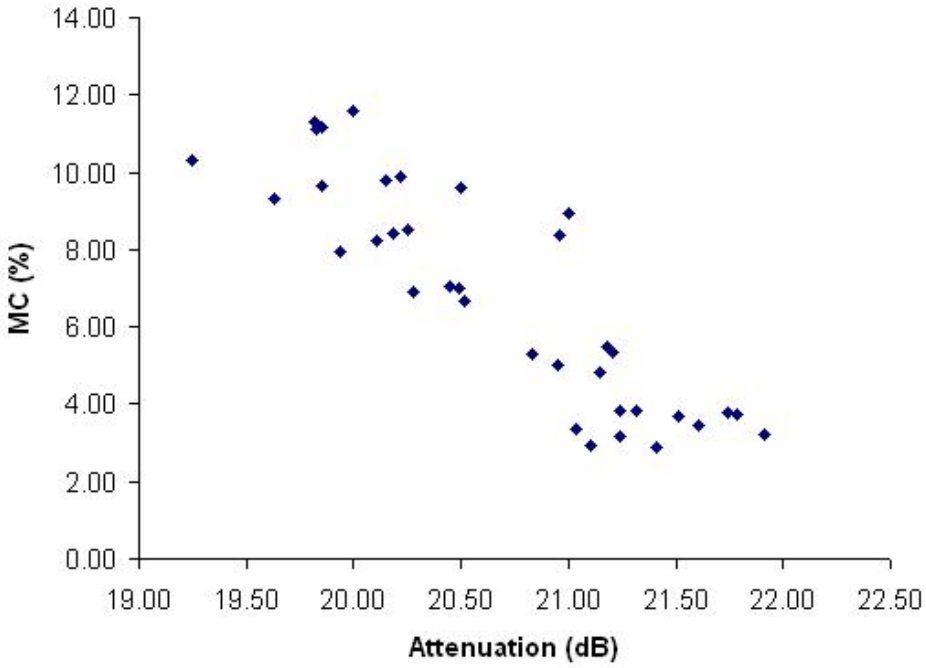

(a)

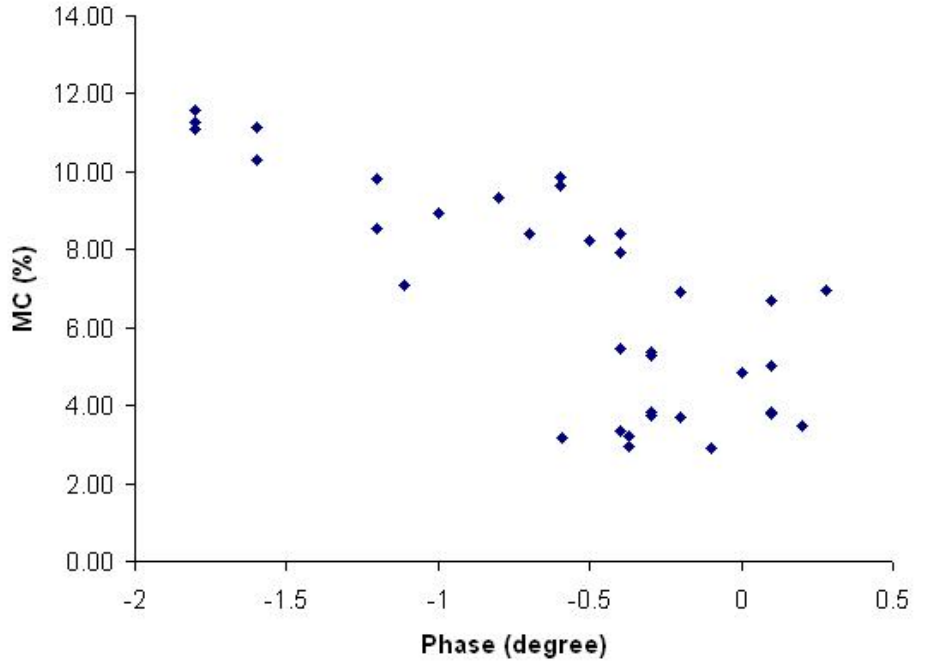

(b)

Figure 4.6. Scatter plot of MC versus (a) attenuation, and (b) phase for relative humidity conditioning method samples.

www.manaraa.com

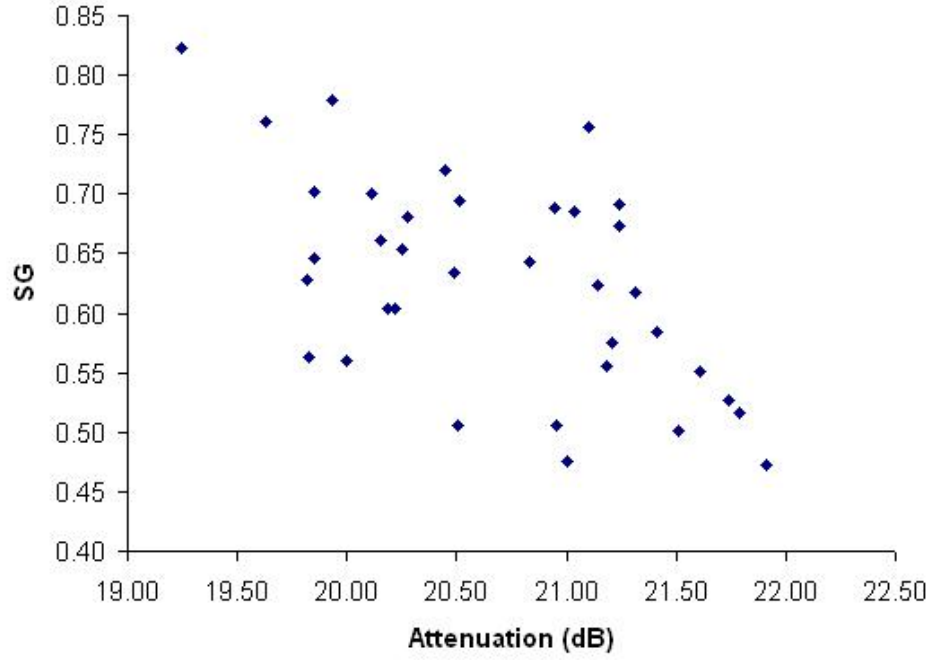

(a)

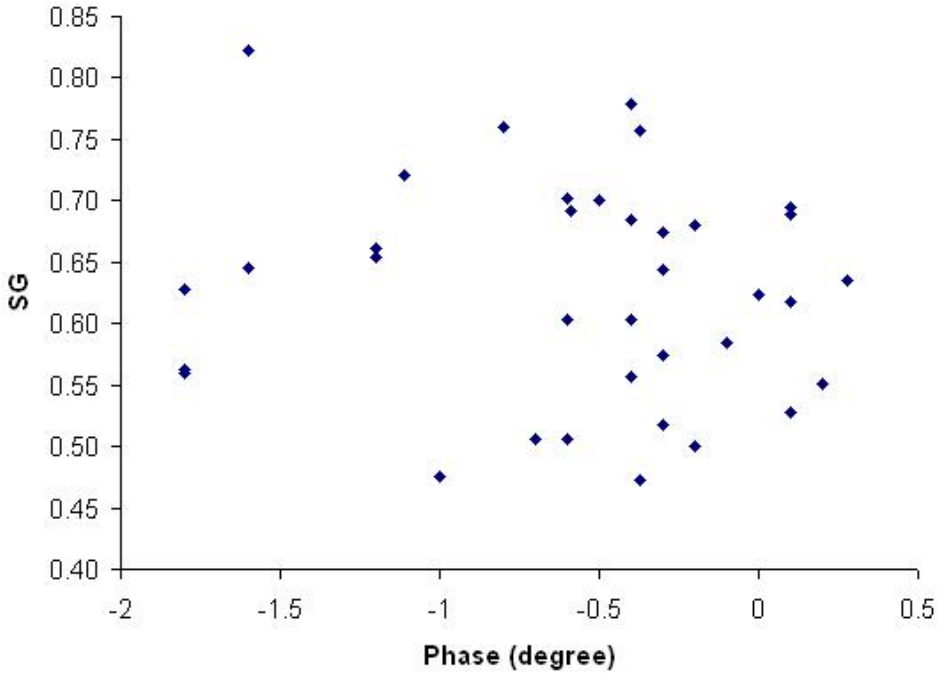

(b)

Figure 4.7. Scatter plot of SG against (a) attenuation and (b) phase for relative humidity conditioning method samples.

www.manaraa.com

Stepwise regression method selected the optimum prediction models for MC and SG. Model 1 and Model 2 are the selected models:

$$MC = -11403 + 1665.637 \times Att - 80.843 \times Att^2 + 1.305 \times Att^3 + 0.571 \times Phase^2 + \varepsilon_1 \quad \text{Model 1}$$

$$SG = 663.656 - 96.342 \times Att + 4.668 \times Att^2 - 0.0754 \times Att^3 - 0.0236 \times Phase^2 + \varepsilon_2 \quad \text{Model 2}$$

Where: MC = moisture content (%)
SG = specific gravity
Att = voltage attenuation (dB)
Phase = phase shift (degree)
$\varepsilon_1, \varepsilon_2$ = error terms

The scatter plot of MC and SG residuals versus predicted MC and SG of the selected models (Figure 4.8) indicated there was no significant non-constancy of the error variance. Figure 4.9 showed the normal probability plot of MC and SG residual. Both of the two plots showed perfectly straight lines, which indicated the residuals were all normally distributed. Hence, the error terms (ε_i) of two models for predicting MC and SG all satisfied the normality assumption.

www.manaraa.com

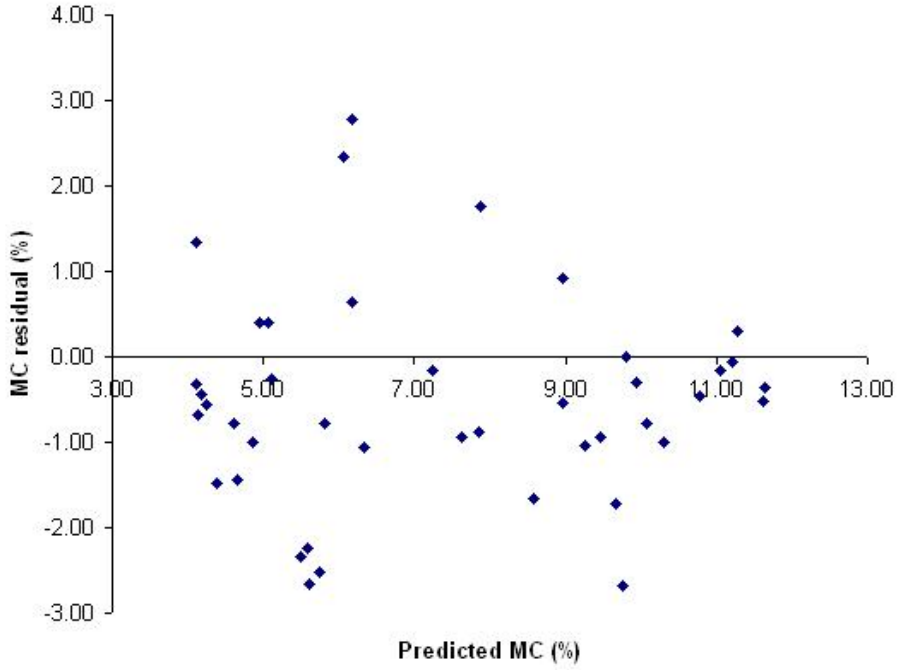

(a)

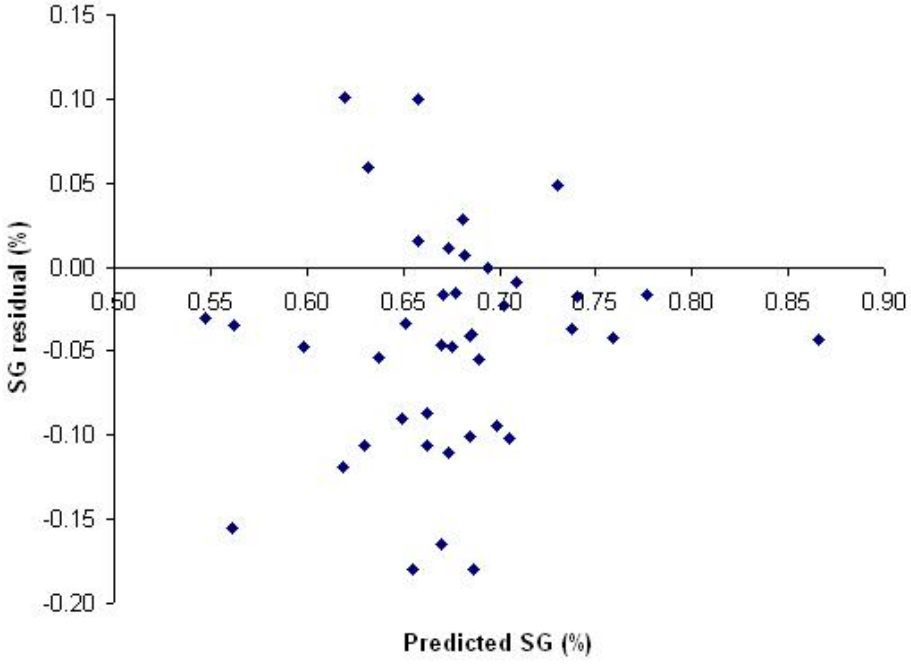

(b)

Figure 4.8. (a) MC and (b) SG residual vs. predicted values of regression equation generation data for relative humidity samples.

www.manaraa.com

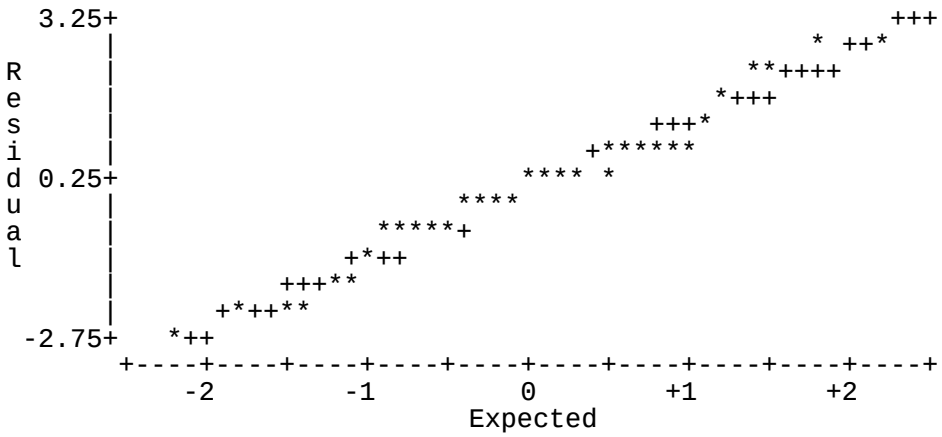

(a) MC residual

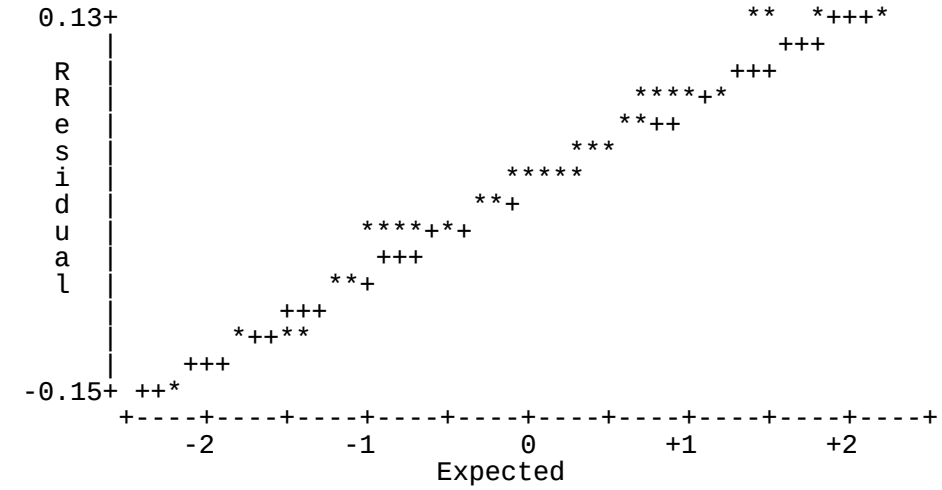

(b) SG residual

Figure 4.9. MC and SG residual normal probability plot for relative humidity conditioning samples.

www.manaraa.com

4.2.1.1 Model validation

Table 4.1 summarizes the regression analysis results for the selected models for both model building and validation data sets. Letters A through E were the coefficients of MC prediction models, and letter F through J were the coefficients of SG prediction models. The first observation was that the differences between the model building and the validation data sets for the PRESS, the SSE, and the R^2 values were relatively small. This indicated that the models generated from the model building data set had the ability to estimate MC and SG with the validation data set. In the case of MC prediction, the validation SSE and MSE values were slightly smaller, which indicated the models from validation data set was slightly more accurate than those from the model-building data set. The similar observation was found for SG regression model. Therefore, the model accuracy of SG prediction with the model from the validation data set was more accurate than the one from the model-building data. The MSPR value of MC prediction was 1.35, which was very close to the MSE value of model-building case. For the SG prediction, the MSRP was very close to the MSE. The closeness of MSRP and MSE indicated the high predictive accuracy of fitted regression models for both MC and SG prediction.

www.manaraa.com

Table 4.1 Results for the linear regression equations for MC and SG prediction of relative humidity conditioning method samples.

Fitted regression equation		Model building data set	Validation data set
MC	A	-11403	-9544.97
	B	1665.64	1401.00
	C	-80.84	-68.29
	D	1.30	1.11
	E	0.57	0.34
	R^2	0.81	0.83
	SSE	60.25	51.90
	PRESS	67.16	56.42
	MSE	1.63	1.40
	MSPR	1.35	
SG	F	663.66	435.06
	G	-96.34	-63.10
	H	4.67	3.06
	I	-0.075	-0.049
	J	-0.02	-0.02
	R^2	0.51	0.48
	SSE	0.176	0.166
	PRESS	0.193	0.189
	MSE	0.00475	0.00448
	MSPR	0.00	

www.manaraa.com

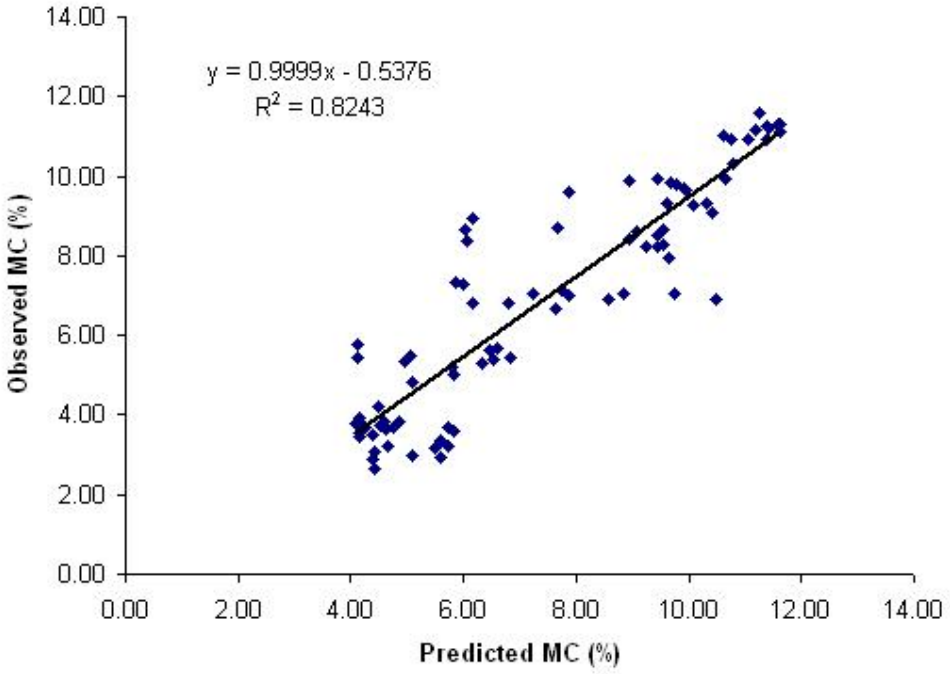

(a)

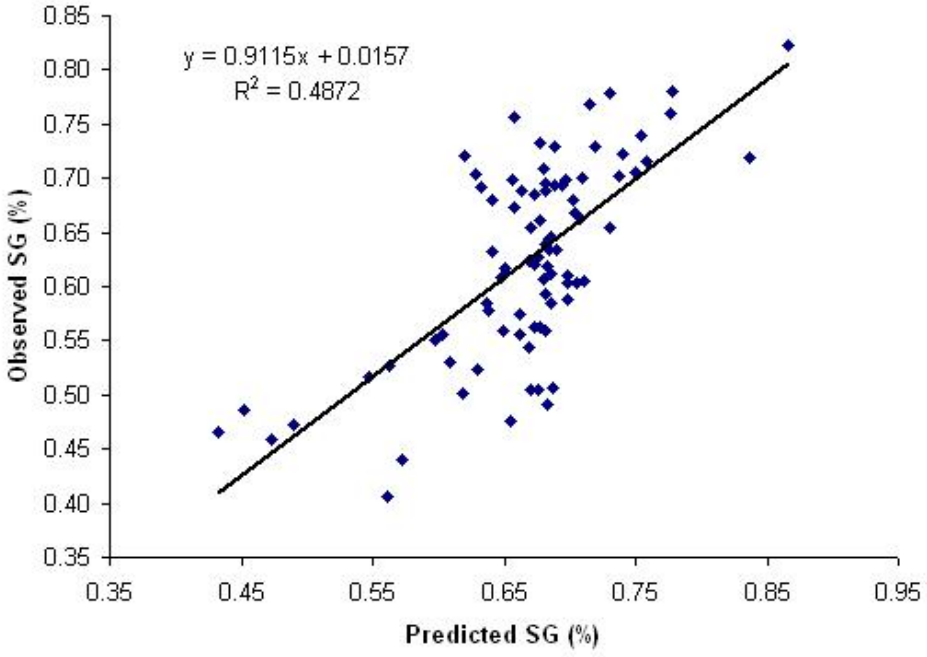

(b)

Figure 4.10. Observed MC against predicted MC (a) and observed SG against predicted SG (b) for relative humidity conditioning method samples.

www.manaraa.com

The scatter plots of observed and predicted MC and SG values were shown in Figure 4.10. It clearly showed that the regression lines for both two regression models were close to a straight line. The scattered points for SG prediction were not spreading as close as MC prediction did. This result was consistent with the fact that MC prediction R^2 values (Table 4.1) were higher that than those of SG prediction. Therefore, it was concluded, for the relative humidity conditioning method samples, the regression model for MC had a better accuracy of prediction than the one for SG.

4.3 Oven-drying conditioning method

4.3.1 Model development

4.3.1.1 Data normality checking

Similar to the model development process of the relative humidity conditioning data set, the normality checking of variables was performed first to the oven-dry data set. Appendix B 2.1 and 2.2 showed the normality test results of model building data set and validation data set of oven-drying conditioning specimens.

Results of the Shapiro-Wilk test indicated that the normality assumption for each variable was held with a p-value grater than 0.05. The normality probability plots for each variable of both model building and validation data set showed straight lines that indicated all the variables were normally distributed.

www.manaraa.com

4.3.1.2 Model selection

One of the two replication samples was randomly assigned number 1 and the other one was assigned number 2. Therefore, half of 246 measured data points were grouped as the model building set, and the rest of 123 data points were grouped as the validation data set.

Figures 4.11 and 4.12 showed the scatter plots of dependent variables (MC and SG) versus predictor variables (phase and attenuation) of the model-building data set. Attenuation showed a curvilinear relationship with both MC and SG. An obvious curvilinear relationship between phase shift and MC was also observed.

www.manaraa.com

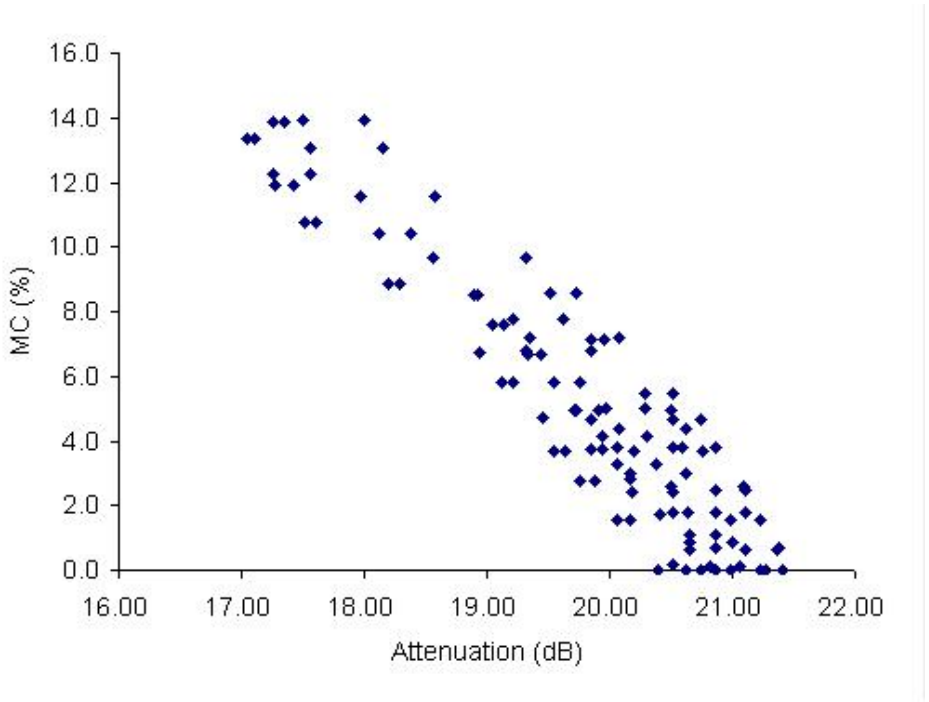

(a)

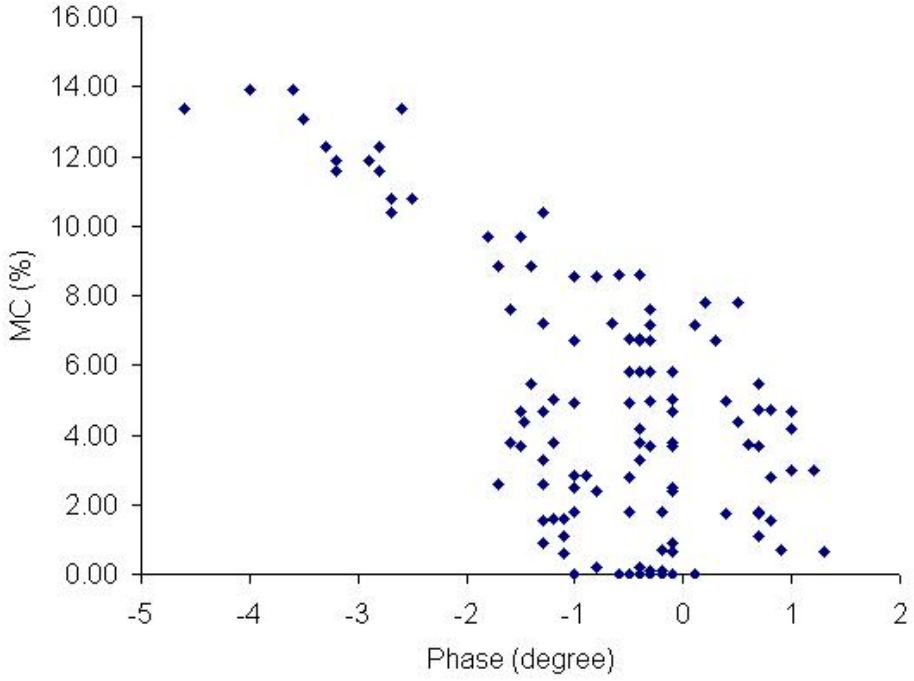

(b)

Figure 4.11. The scatter plots of MC against (a) attenuation and (b) Phase, of oven-drying conditioning samples.

www.manaraa.com

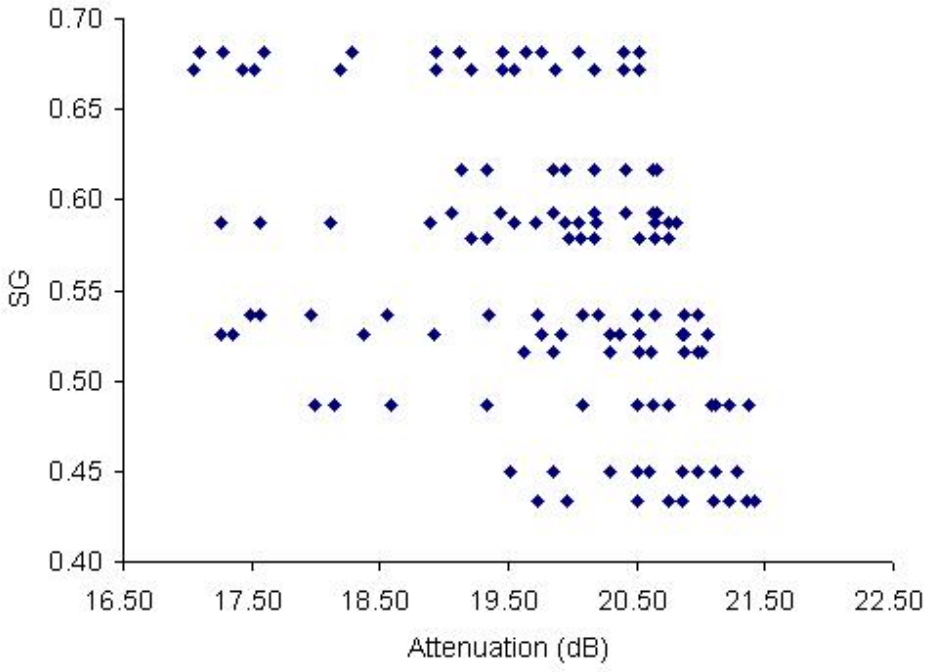

(

a)

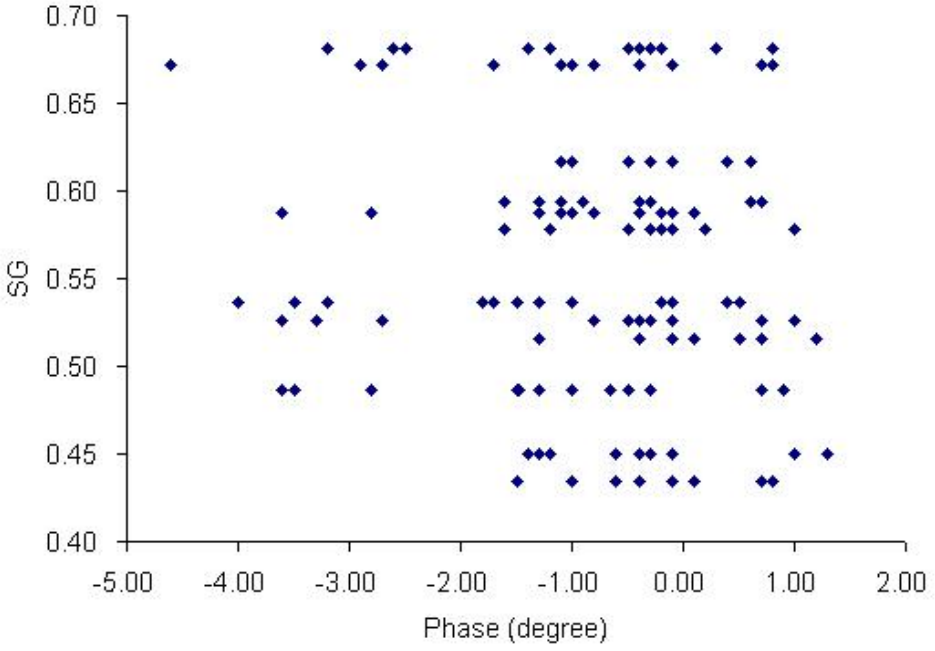

(b)

Figure 4.12. The scatter plot of SG against (a) phase and (b) attenuation of oven-drying conditioning samples.

www.manaraa.com

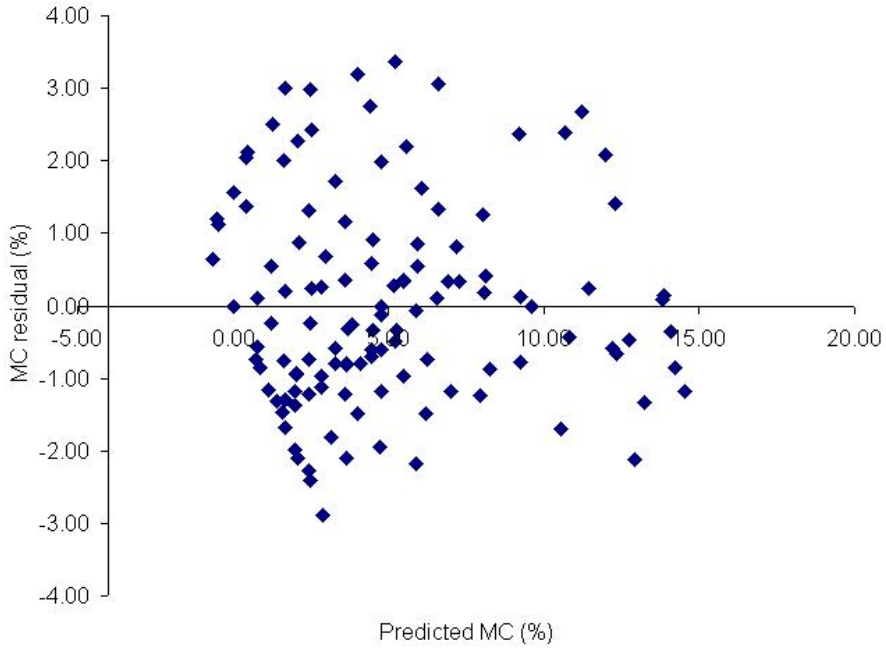

(a) MC Residual

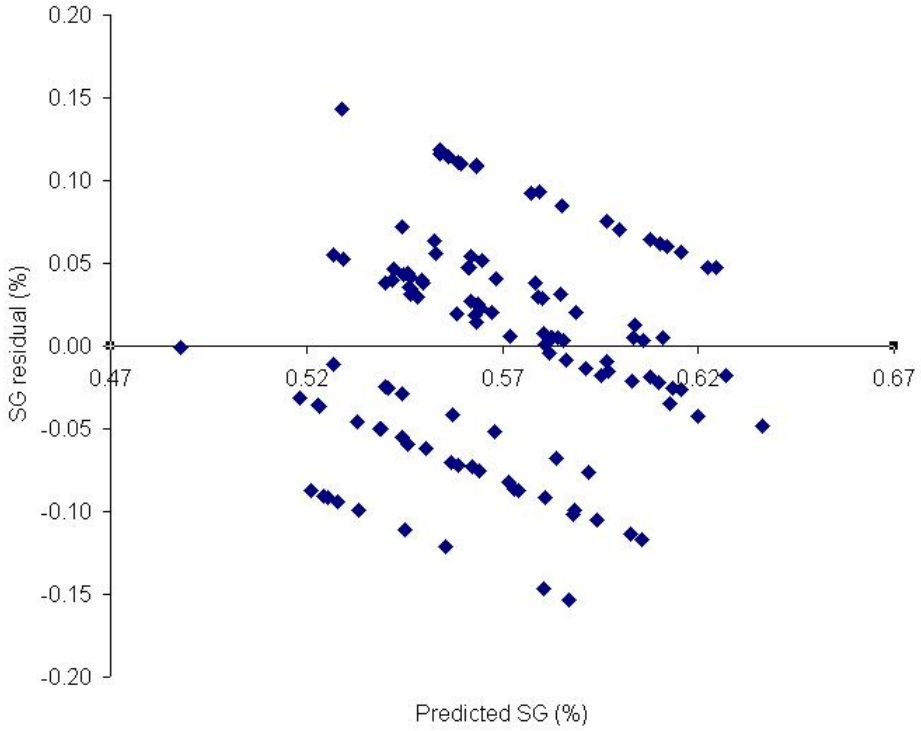

(b) SG residual

Figure 4.13. MC and SG residual vs. predicted values of regression equation generation data for oven-drying conditioning samples.

www.manaraa.com

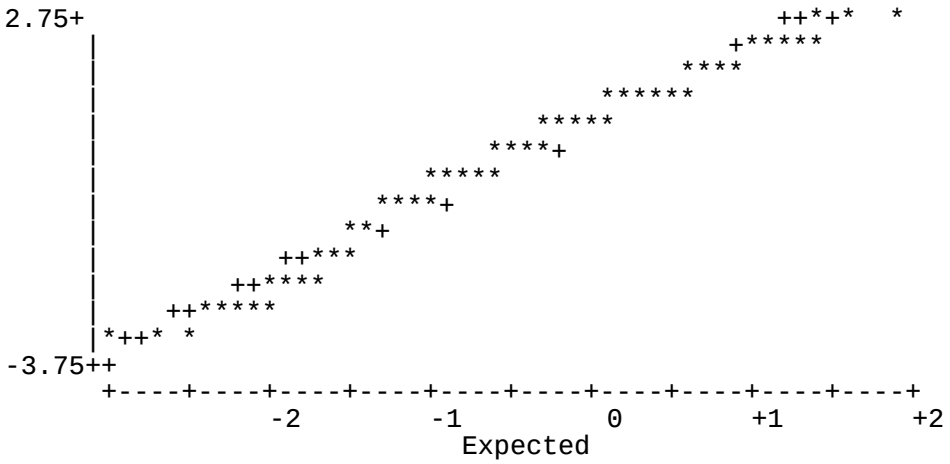

(a) MC residual

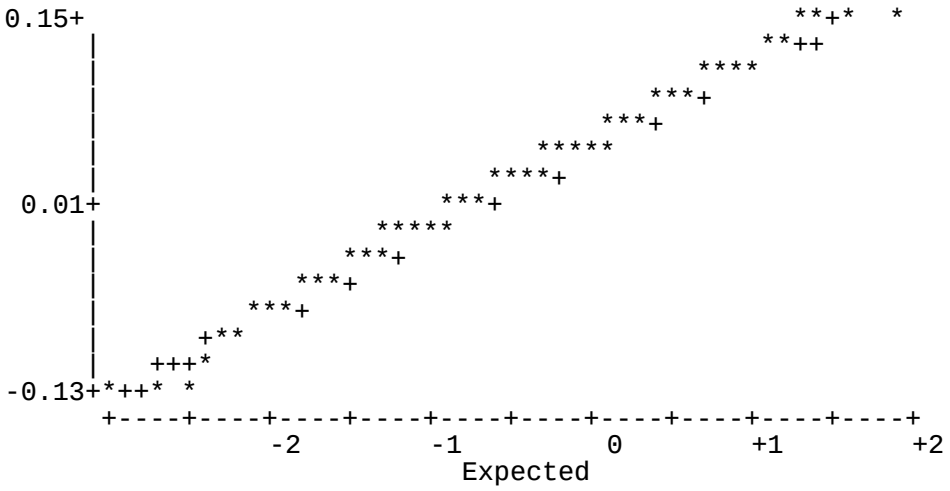

(b) SG residual

Figure 4.14. MC and SG residual normal probability plot of oven-drying conditioning samples.

www.manaraa.com

However, the correlation between phase shift and SG was not obvious. In this way, the scatter plots of each pair of variables can be used to help deciding the regression models in terms of orders of the predictor variables.

The stepwise regression method was used in this research. Models 3 and 4 were selected and tested for the further validation processes:

$$MC = -2882.06 + 448.43 \times Att - 23.00 \times Att^2 + 0.39 \times Att^3 + 0.26 \times Phase^2 + \varepsilon_1 \quad \text{Model 3}$$

$$SG = 139.71 - 21.64 \times Att + 1.12 \times Att^2 - 0.02 \times Att^3 - 0.01 \times Phase^2 + \varepsilon_2 \quad \text{Model 4}$$

Figure 4.14 shows the normal probability plot of MC and SG residual. Both of the two plots are showing perfectly straight, which is indicating the residuals are all normally distributed. Hence the error terms (ε_i) of two models for predicting MC and SG are all following the normality assumption.

4.3.1.3 Model validation

Regression coefficients for the selected models were estimated with the validation data set, and then those coefficients were compared for consistency with the coefficients from the model building data set.

Table 4.2 summarized the regression analysis results of the selected models for both the model building and the validation data set for the oven-drying conditioning method samples. The differences between the model building and the validation data sets were relatively small for all the PRESS, the SSE, and the R^2 values. This indicated that the models generated from the model-building data set had the ability to estimate MC and SG with validation data set. In the case of MC prediction, the validation SSE

www.manaraa.com

Table 4.2 Results for the linear regression equations for MC and SG prediction of oven-drying conditioning method samples.

Fitted regression equation		Model building data set	Validation data set
MC	A	-2882.05781	-1731.39356
	B	448.42594	273.17336
	C	-23.00072	-14.13863
	D	0.38971	0.24087
	E	0.25955	0.23811
	R^2	0.8970	0.8802
	SSE	207.52676	241.39798
	PRESS	218.85230	254.40551
	MSE	1.75870	2.04575
	MSPR	2.26	
SG	F	139.71050	66.27797
	G	-21.63863	-10.31165
	H	1.12144	0.54053
	I	-0.01936	-0.00946
	J	-0.01014	-0.00961
	R^2	0.3024	0.3106
	SSE	0.42422	0.40794
	PRESS	0.45374	0.43213
	MSE	0.00360	0.00346
	MSPR	0.01	

www.manaraa.com

and MSE values were slightly smaller than the model building ones, which indicated the models from validation data set were slightly more accurate than those from the model-building data. There was no obvious difference between SSE and MSE values for SG prediction. Therefore, the model accuracy of SG prediction with models from both the model-building data set and the validation data set were almost the same. The MSPR value of MC prediction was 1.94, which was fairly close to 1.74414, the MSE value of model-building case. So does for the SG prediction, the MSRP was 0.01, the MSE was 0.00333. The closeness of MSRP and MSE indicated the predictive accuracy of fitted regression models for both MC and SG.

The scatter plots of observed and predicted MC and SG value were shown in Figure 4.15 (a) and (b). The regression lines for both two regression models were close to a straight line for MC prediction. The scattered points for SG prediction were not spreading as close as MC prediction does. This was consistent with the fact that MC prediction R^2 values (Table 4.2) were higher that than those of SG prediction. Therefore it was concluded that for the oven-drying conditioning method samples, the regression models for MC has a better accuracy of prediction than those for SG.

www.manaraa.com

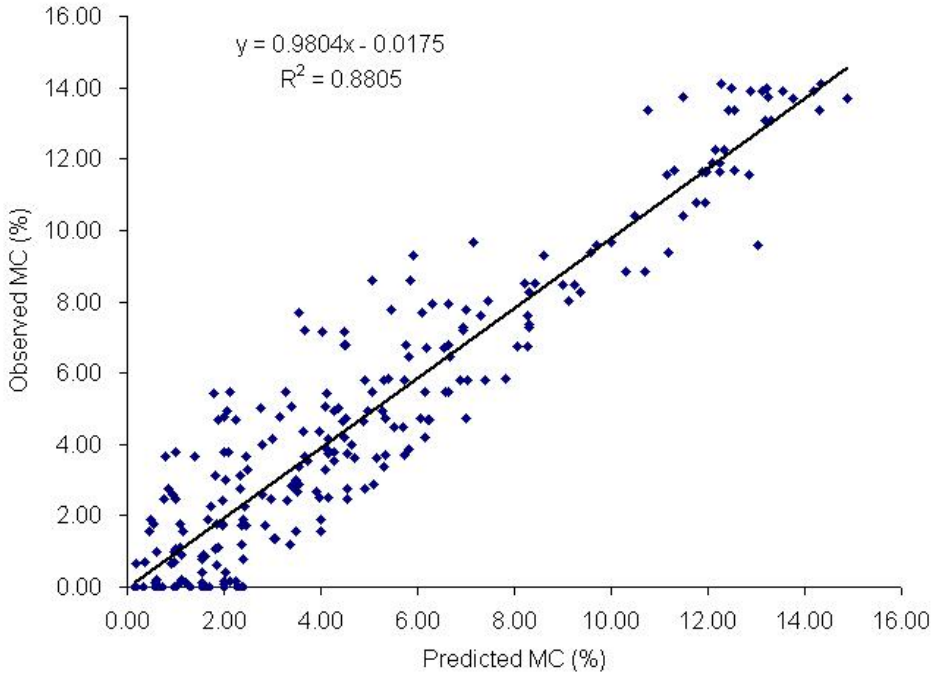

(a)

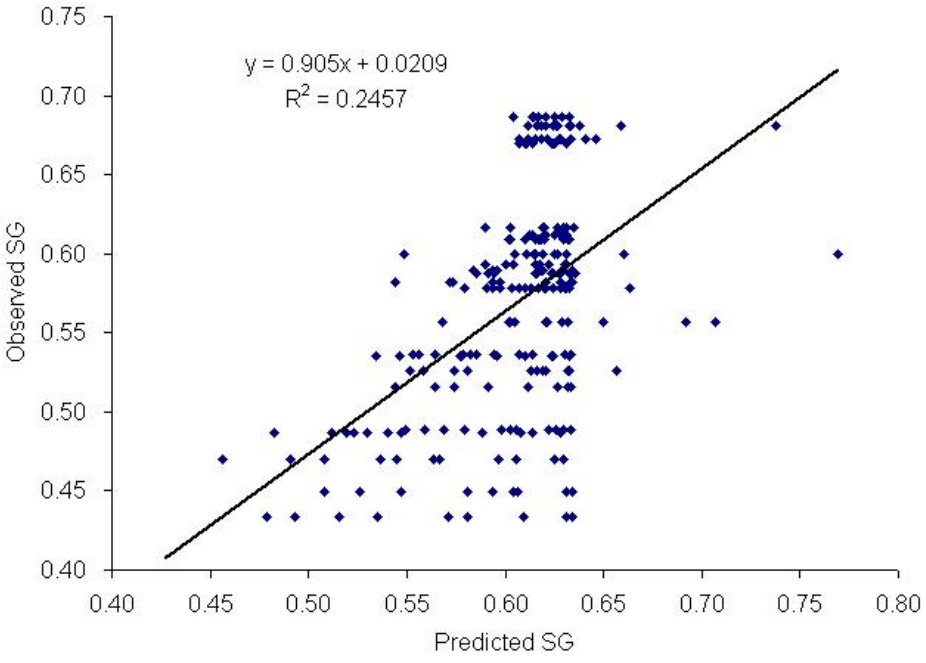

(b)

Figure 4.15. (a) Observed MC against predicted MC, and (b) Observed SG against predicted SG for oven-drying conditioning samples.

www.manaraa.com

4.4 Model comparison

Table 4.3 summarized the final models for MC conditioning methods of relative humidity conditioning and oven-drying conditioning, respectively. Figures 4.16 and 4.17 showed the 3D plots of these prediction models. The attenuation ranged from 19.25 to 21.25 dB. The phase ranged from -1.5 to 2.5 degrees. By checking the shapes of the plotted 3D surfaces of the two figures, different behaviors were obvious between these two models.

Table 4.3. Final models of MC and SG perdition for different conditioning methods.

Conditioning method	Prediction models
Relative humidity conditioning	$MC = -11403 + 1665.64 \times Att - 80.84 \times Att^2 + 1.31 \times Att^3 + 0.57 \times Phase^2$
	$SG = 663.67 - 96.34 \times Att + 4.67 \times Att^2 - 0.075 \times Att^3 - 0.024 \times Phase^2$
Oven drying conditioning	$MC = -2882.06 + 448.43 \times Att - 23.00 \times Att^2 + 0.39 \times Att^3 + 0.26 \times Phase^2$
	$SG = 139.71 - 21.64 \times Att + 1.12 \times Att^2 - 0.02 \times Att^3 - 0.01 \times Phase^2$

To get a better view of the comparison between the models, the 2D projection of MC and SG prediction models were plotted in Figure 4.18 and 4.19, respectively.

In the MC vs. Phase projection (Figure 4.18(a)), most of MC predicted values from relative humidity model were higher than those of oven-drying model, but still had some overlaps within the phase shift changing ranges. The trend of MC values was always decreasing for relative humidity condition, while the oven-drying conditioning's were decreasing first between -2 to 0 degree phase region. Then most part of the MC predictions overlapped when phase was higher than 0 degree.

www.manaraa.com

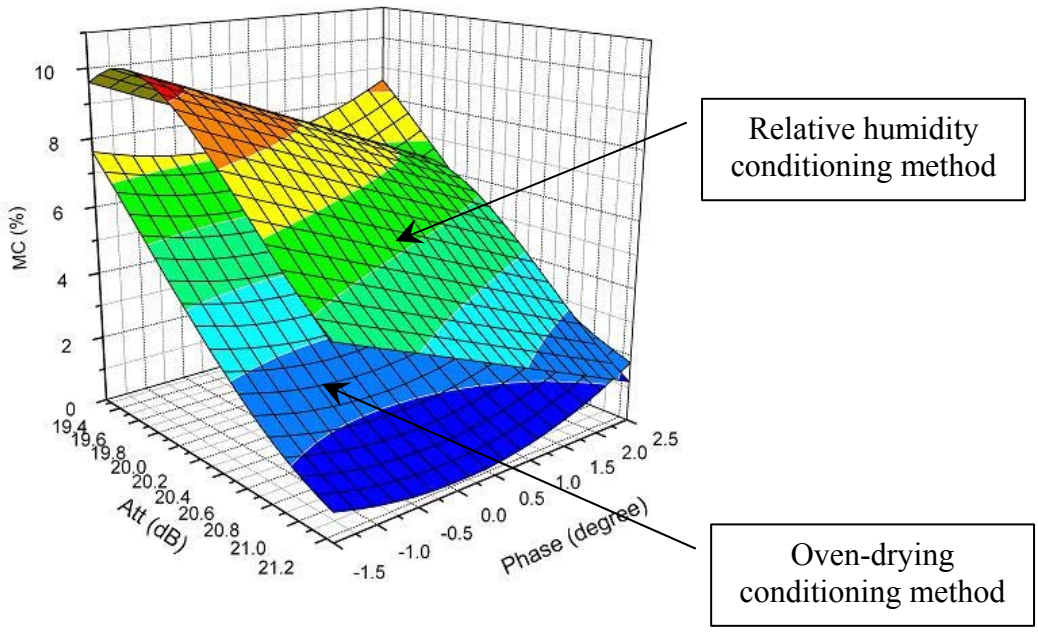

Figure 4.16. 3D plots of MC prediction models for (a) relative humidity conditioning method, and (b) oven-drying conditioning method.

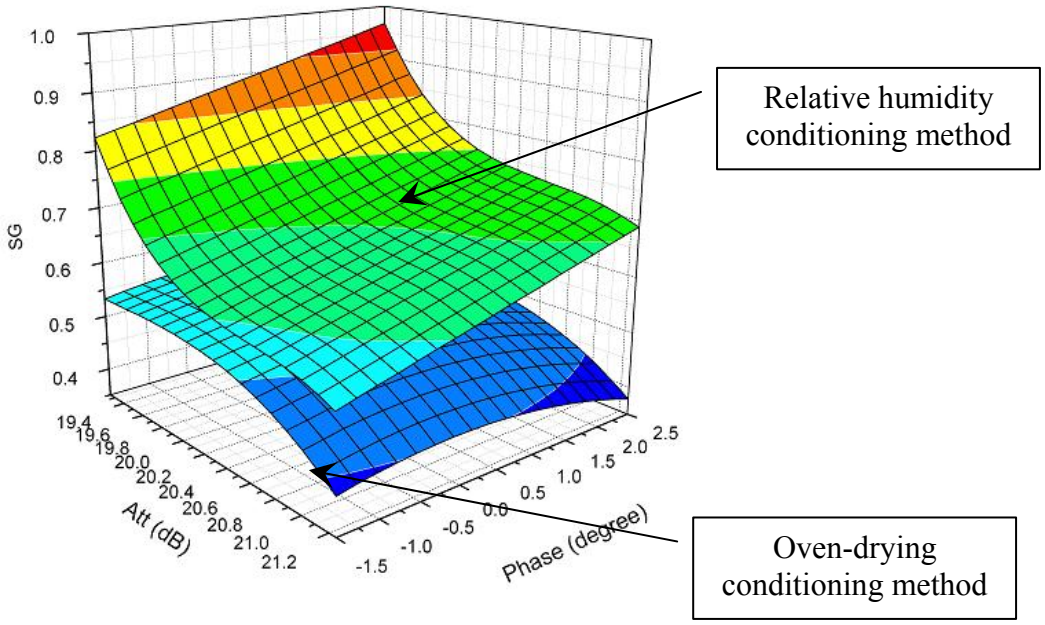

Figure 4.17. 3D plots of SG prediction models for (a) relative humidity conditioning - method, and (b) oven-drying conditioning method.

www.manaraa.com

In the MC vs. Att projection (Figure 4.18 (b)), the relative humidity conditioning method model prediction values were also higher than those of oven-drying conditioning method. However, the overlaps of MC prediction values between these two conditioning methods were far less than those of MC vs. Phase projection. In both Figure 4.19(a) and (b), all the SG prediction values of models from relative humidity conditioning method were higher than those from oven-drying conditioning method.

Therefore, the behavior of the MC an SG prediction models generated from relative humidity conditioning method were different from that of oven-drying conditioning method. The two moisture conditioning methods might produce different dielectric response in RF scanning test even for the same OSB material. In the process of RF evaluation of OSB MC and SG, the specimen conditioning procedures should be carefully kept consistency; otherwise the results will not be accurate.

www.manaraa.com

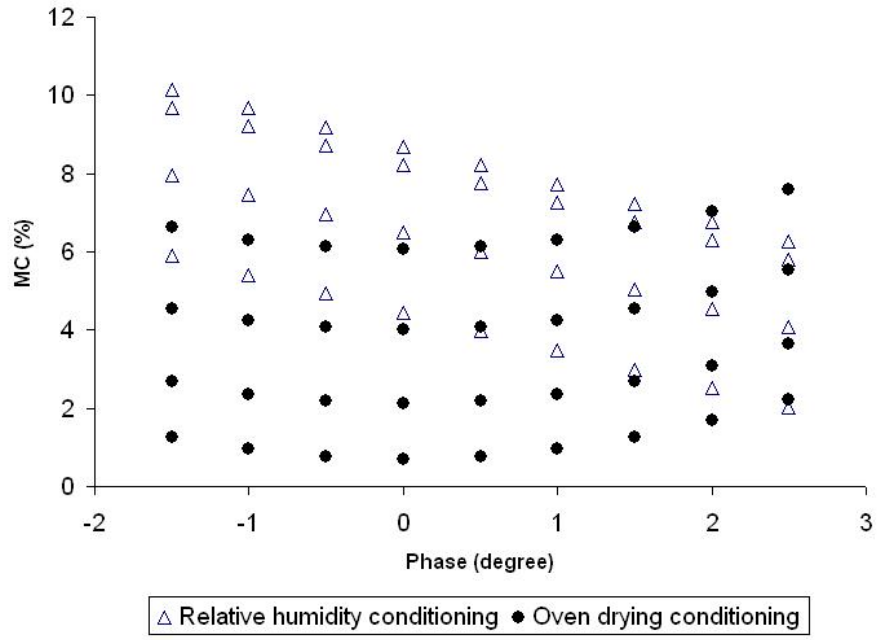

(a)

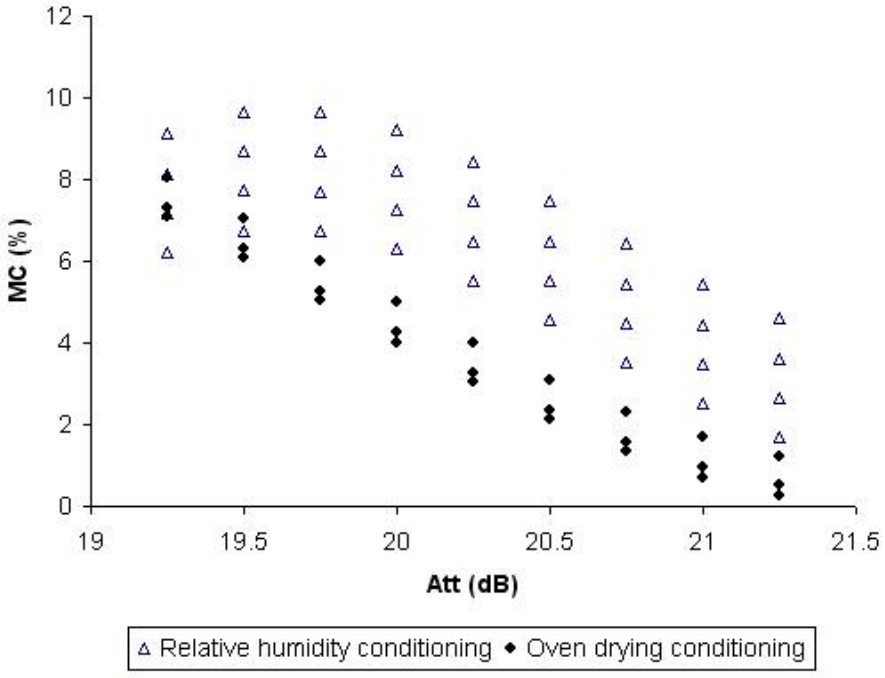

(b)

Figure 4.18. 2D projections of MC prediction models comparison between relative humidity conditioning method and oven-drying conditioning method for (a) MC vs. phase cross section, and (b) MC vs. Att cross section.

www.manaraa.com

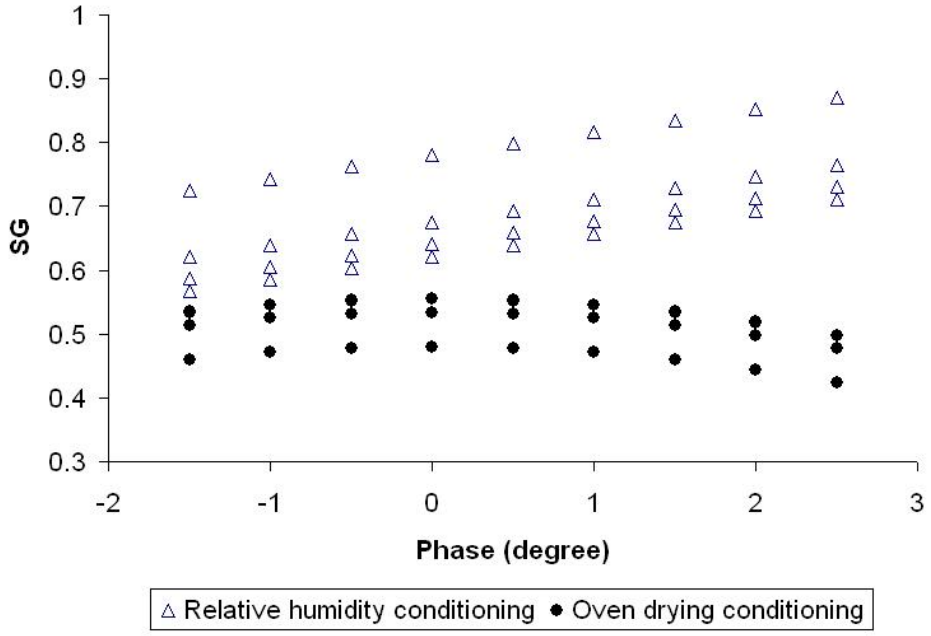

(a)

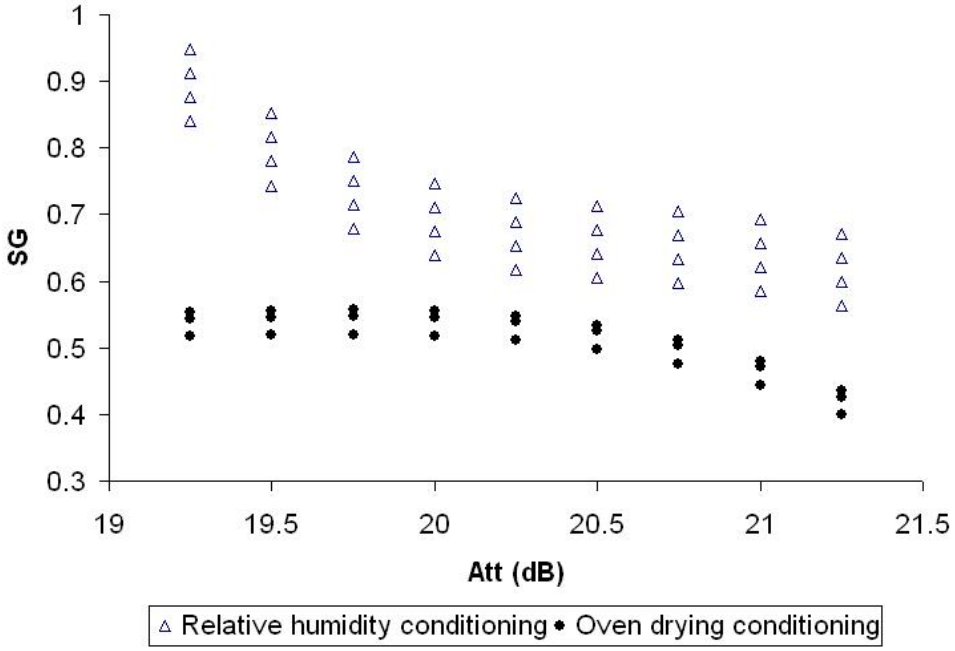

(b)

Figure 4.19. 2D projections of SG prediction models comparison between relative humidity conditioning and oven-drying conditioning method for (a) MC vs. phase cross section, and (b) MC vs. Att cross section.

www.manaraa.com

CHAPTER V

SUMMARY AND CONCLUSION

In this research, the radio frequency (RF) scanning method was evaluated numerically and experimentally as a NDE tool to measure the MC and SG of OSB panel products. The MLR method was used to develop regression models including significant RF signal responses attenuation and phase to estimate MC and SG of OSB.

The numerical simulation method assisted in developing RF sensor geometry. The effective electric filed strength (E) distribution patterns were visualized to help determine the optimum sensor shape, size and effective sensor scanning area. Square shaped 4" wide parallel plate sensors were chosen based on simulation results.

The sensor size and sensor spacing studies were conducted experimentally using RF scanning device. The experimental results using 4" wide sensors matched the one from the simulation. The sensor spacing study showed that the optimum distance between edges of two pair sensors (sending and receiving) was 1", which is useful information for design of multiple sensor scanning device.

. Seven levels of MC and 6 levels of SG OSB specimens were prepared for each of two different MC conditioning methods, relative humidity conditioning method and oven-drying conditioning method, respectively. The scanning results in terms of RF signal responses to MC and SG of studied OSB materials were used to derive MC and

www.manaraa.com

SG prediction models as functions of significant responses attenuation and phase. The best models were then selected using the multiple linear regression method. The comparisons between the two models derived from different MC conditioning method were conducted.

The following conclusions can be made from this study: (1) The RF scanning method is an effective technique to nondestructively evaluate the OSB MC and SG; (2) MC and SG prediction models derived from RF scanning data using the procedure conducted in this study can be used to estimate MC and SG of OSB composites simultaneously; (3) the MC conditioning method is a significant factor to OSB composite RF responses, a different conditioning method might produce different MC & SG prediction results. Further research along these lines could eventually lead to the development of a multiple sensors RF scanning device which could be used as in-line real-time MC and SG detector for the OSB industry.

www.manaraa.com

LITERATURE CITED

Adair, C. 2004. Regional production and market outlook: Structural panels and Engineered Wood Products 2004-2009. Publication E170. APA-The Engineered Wood Assoc., Tacoma, WA.

American Society for Testing Materials. 2002. Standard partice for maintaining constant relative humidity by means of aqueous solutions. ASTM E104-02. Philadelphia, PA.

American Society for Testing Materials. 2004. Standard guide for moisture conditioning of wood and wood-based materials. ASTM D4933-99 (Reapproved 2004). Philadelphia, PA.

Bulleit, W. M., and R. H. Falk. 1985. Modeling stress wave passage times in wood utility poles, Wood Sci. Tech. 19:183-191.

Brashaw, B. K., R. J. Ross, R. J. and P. R. Roy. 1996. Stress wave nondestructive evaluation of green veneer: southern yellow pine and Douglas fir. Proceedings of the international society for optical engineering: Nondestructive evaluation of materials and composites. 2944: 296-306.

EN300 2001. Standard for manufacturing structural wood composite panel. European Committee for Standardization, Brussels.

Greenspan, L. 1977. Humidity fixed points of binary saturated aqueous solutions." J. Res. Nat. Bur. Stand. 81A: 89–96.

Gerhards, C. C. 1982. Effect of moisture content and temperature on the mechanical properties of wood: an analysis of immediate effects. Wood and Fiber Sci. 14:4-36.

Halligan, A. F. and A. P. Schniewind. 1974. Prediction of particleboard mechanical properties at various moisture contents. Wood Sci. and Tech. 8:68-78.

Hansson, L., N. Lundgren, A. L. Antti and O. Hagman 2006. Finite element modeling (FEM) simulation of interactions between wood and microwaves. J. Wood Sci. 52:406-410.

www.manaraa.com

Hoover, W. L., M. O. Hunt, R. C. Lattanzi, J. H. Bateman and J. A. Youngquist. 1992. Modeling mechanical properties of single-layer, aligned, mixed-hardwood strand panels. Forest Prod. J. 42(5): 12-18.

Howard, J. L. 2006. US Forest products annual market review and prospects, 2002-2006. USDA Forest Service. Madison, WI.

Jazayeri, S. and Ahmet, K. 2000. Detection of transverse moisture gradients in timber by measurements of capacitance using a multiple-electrode arrangement. Forest Prod. J. 50(11/12):27-32.

James, W. L. 1975. Dielectric properties of wood and hardboard: variation with temperature, frequency, moisture content, and grain orientation. Madison, WI: U.S. Department of Agriculture, Forest Service, Forest Products Laboratory.

James, W. L. 1988. Electric moisture meters for wood. Gen. Tech. Rep. FPL–GTR–6. Madison, WI: U.S. Department of Agriculture, Forest Service, Forest Products Laboratory.

Jha, S.N., Chopra S. and Kingsly A. R. P. 2007. Modeling of color values for nondestructive evaluation of maturity of mango. J. Of food engineering, 78:22-26.

Jin, J. 2002. The finite element method in electromagnetics. Wiley, New York

Kabir, M. F., W.M. David, K. Khalid and H. A. A. Sidek. 1998. Dielectric and ultrasonic properties of rubber wood. Effect of moisture content, grain direction and frequency. Holz als Roh-und Werkstoff, 56:223-227.

Khalid, K. B., M. F. Kabir, W. M. Dand and H. A. A. Sidek. 1999. Multi-component mixture modeling for the dielectric properties of rubber wood at microwave frequencies. Holtzforschung 53:662-668

Kutner M. H, C. J. Nachtsheim, J. Neter and L. William. 2005. Applied linear statistical models, 5th edition. McGraw-Hill, Irwin, CA.

Mendenhall, W. and T. Sincich. 1989. A second course in business statistics: regression analysis. Dellen Pub. Comp. San Francisco, CA.

Muller, U., A. Sretenovic, W. Gindl, M. Grabner, R. Wimmer and A. Teischinger. 2004. Effects of macro- and micro-structural variability on the shear behavior of softwood. IAWA Journal, 25(2): 231-243.

Olin, B. D. and W. Q. Meeker. 1996. Applications of statistical methods to nondestructive evaluation. Technometrics, 38(2): 95-130.

www.manaraa.com

Palacios, P., L. G. Esteban, A. Guindeo, F. G. Fernandez, A. F. Canteli and N. Navarro. 2008. Variation of impact bending in the wood of *Pinus sylvestris* L. in relation to its position in the tree. 2008. Forest Prod. J. 58(3):55-60.

Parker, R. S. and F. C. Beall. 1986. Method of measuring moisture content of dielectric materials. U.S. Patent No. 4,580,223.

Reddy. J. N. 1993. An introduction to the finite element method, 2nd edition. McGraw-Hill, New York, NY.

Resch, H. and B. A. Ecklund. 1964. A statistical analysis of the variability in the drying rate of redwood. Forest Prod. J. 14(9): 430-434.

Rice, R. W., P. H. Steele and L. Kumar. 1992. Detecting knots and voids in lumber with dielectric sensors. Industrial Metrology 2. Elsevier Sci. Pub. 315 pp.

Ross, R. J. and R. F. Pellerin. 1988. NDE of wood-based composites with longitudinal stress waves. Forest Prod. J. 38(5):39-45.

SAS Institute (2006) SAS 9.1.3. SAS Institute. Cary, NC.

Simola K. and U. Pulkkinen. 1998. Models for non-destructive inspection data. Reliability Engineering and System Safety. 60(1998): 1-12.

Sobue, N. 2000. Measurement of moisture gradient in wood by electrode scanning moisture analysis (ESMA). In Proc. of the 12th International Symposium on Nondestructive Testing of Wood. September 13-15, 2000. University of Western Hungary, Sopron, Hungary.

Steele, P. H. and J. Cooper. 2004. Moisture and density detector (MDD). U.S. Patent 6,784,671. U.S. Patent Office, Washington, DC.

Steele, P. H. and L. Kumar. 1996. Detector for heterogeneous materials. US patent 5,585,732. US Patent office, Washington, DC.

Suchsland, O. 1962. The density distribution in flake boards. Michigan Quarterly Bulletin. 45(1):104-121.

Suchsland, O. 1973. Hygroscopic thickness swelling and related properties of selected commecial particleboards. Forest Prod. J. 23(7):26-30.

Suchsland, O. and H. Xu. 1989. A simulation of the horizontal density distribution in a flakeboard. Forest Prod. J. 39(5):29-33.

www.manaraa.com

Suchsland, O. and H. Xu. 1991. Model analysis of flakeboard variables. Forest Prod. J. 41(11/12):55-60.

Sweeting, T. 1995. Statistical models for nondestructive evaluation. International Statistical Review, 63(2): 199-214.

Thomson, W. T. 1981. Theory of vibration with applications, Second Edition. Prentice-Hall, Inc., Englewood Cliffs, NJ, USA,

Torgovnikov, G. I. 1993. Dielectric Properties of Wood and Wood-Based Materials. Springer-Verlag. 196 pp.

USDA Forest Service, Forest Products Laboratory. 1999. Wood Handbook: Wood as an Engineering Material. Gen. Tech. Rept. FPL-GTR-113. Forest Prod. Soc., Madison, WI. 464 pp.

Vermaas, H. F. 1974. Dielectric properties of Pinus pinaster as a function of its alcohol-benzenz-soluble content. Wood Science, 6(4):363-367.

Von Hippel, A. R. 1954. Dielectric materials and applications. MIT, New York.

Vun, R. Y. and Q. Wu. 2003. Ultrasonic characterization of structural properties of oriented strandboard: contact vs. non-contact methods. Wood and Fiber Sci. 35(3):381-396.

Wagner, E. D. 1996. Moisture detection circuit. US patent. 5,486,815. US Patent office, Washington, DC.

Walker, J. C. F. 2006. Primary Wood Processing: Principles and Practice. Springer, Dordrecht. 596 pp.

Wang, S. Q. and P. M. Winistorfer. 2003. Monitoring resin cure during particleboard manufacture using a dielectric system. Wood and Fiber Sci. 35(4): 532-539.

Watkinson, P. J. and N. L. van Gosliga. 1990. Effect of humidity on physical and mechanical properties of New Zealand wood composites. Forest Prod. J. 40(7/8):15-20.

Wilcox, W. W. 1988. Detection of early stages of wood decay with ultrasonic pulse velocity. Forest Prod. J. 35(5):68-73.

Williamson, T.G. (editor) 2002. Engineered wood handbook. APA, McGraw-Hill, New York.

Wolcott, M. P. and T. G. Rials. 1995. In-situ cure monitoring of isocyanate adhesives using microdielectric analysis. Forest Prod. J. 45(2):72-77.

www.manaraa.com

Wu, Q. and O. Suchsland. 1997. Effect of moisture on the flexural properties of commercial oriented strandboard. Wood and Fiber Sci. 29(1):47-57.

Young, T. M., L. B. Shaffer, F. M. Guess, H. Bensmail and R. V. Leon. 2008. A comparison of multiple linear regression and quantile regression for modeling the internal bond of medium density fiberboard. Forest Prod. J. 58(4): 39-48.

Zhang, S. Y., G. Nepveu and F. Mothe. 1994. Modeling intratree wood shrinkage in European oak by measuring wood density. Forest Prod. J. 44(10):42-46.

www.manaraa.com

APPENDIX A

ORIENTED STRAND BOARD PROCESSING CALCULATIONS

www.manaraa.com

Table A.1. Oriented strand board processing calculations for 35lb/ft^3 target density, surface layer.

Target board density (lb/ft^3)	= 35 lb/ ft^3
Nominal board volume (ft^3)	= 30 in × 30 in × 0.3 in = 270 in^3 = 0.1563 ft^3
Board weight (lb)	= 35 lb/ ft^3× 0.1563 ft^3= 5.47 lb
Board additive: water(%) = EMC	= 8 %
Face resin solid content (%)	= 50 %
Resin solids required (%)	= 3 %
Dry furnish weight (lb)	= 5.47 × (1-wax-resin-additives)
	= 5.47 × (1-0.01-0.03-0.08) = 4.430
Total resin weight (lb)	= (4.43 lb × 3)/50 = 0.266 lb
Wax solids content (%)	= 50 %
Was solids required (%)	= 1 %
Total wax weight (lb)	= (dry furnish weight × wax required)/wax solids
	= (4.430 × 1)/50 = 0.089
Furnish moisture content (%)	= 4%
Mat furnish weight (lb)	= dry furnish weight/(1-furnish MC)
	= 4.430 lb/(1-0.04) = 4.614 lb
Furnish excess factor	= 10% per board = 1.10
	(for furnish loss during blending and mat forming)

Required material weights for surface layer:

	Mat solid wt.	Mat water wt.	Mat wt.	Blend wt (Mat wt.*1.1)
Furnish (lb)	3.797	0.158	3.955	4.351
Resin (lb)	0.114	0.076	0.190	0.209
Wax (lb)	0.044	0.032	0.076	0.084
Total (lb)	3.955	0.266	4.221	4.643

www.manaraa.com

Table A.2. Oriented strand board processing calculations for 35lb/ ft^3 target density, core layer.

Target board density (lb/ft^3)	= 35 lb/ft^3
Nominal board volume (ft^3)	= 30 in × 30 in × 0.2 in = 180 in^3= 0.1042 ft^3
Board weight (lb)	= 35 lb/ ft^3× 0.1042 ft^3= 3.65 lb
Board additive: water(%) = EMC	= 8 %
Core resin solid content (%)	= 60 %
Resin solids required (%)	= 3 %
Dry furnish weight (lb)	= 3.65 × (1-wax-resin-additives)
	= 3.65 × (1-0.01-0.03-0.08) = 2.953 (lb)
Total resin weight (lb)	= (2.953 lb × 3)/60 = 0.148 lb
Wax solids content (%)	= 50 %
Was solids required (%)	= 1 %
Total wax weight (lb)	= (dry furnish weight × wax required)/wax solids
	= (2.953 × 1)/50 = 0.059
Furnish moisture content (%)	= 4%
Mat furnish weight (lb)	= dry furnish weight/(1-furnish MC)
	= 2.953 lb/(1-0.04) = 3.076 lb
Furnish excess factor	= 10% per board = 1.10
	(for furnish loss during blending and mat forming)

Required material weights for core layer:

	Mat solid wt.	Mat water wt.	Mat wt.	Blend wt (Mat wt.*1.1)
Furnish (lb)	2.953	0.123	3.076	3.384
Resin (lb)	0.089	0.059	0.148	0.162
Wax (lb)	0.034	0.025	0.059	0.065
Total (lb)	3.076	0.207	3.283	3.611

www.manaraa.com

Table A.3. Oriented strand board processing calculations for 40lb/ ft^3 target density, surface layer.

Target board density (lb/ft^3)	= 40 lb/ft^3
Nominal board volume (ft^3)	= 30 in × 30 in × 0.3 in = 270 in^3= 0.1563 ft^3
Board weight (lb)	= 40 lb/ft^3 × 0.1563 ft^3= 6.25 lb
Board additive: water(%) = EMC	= 8 %
Face resin solid content (%)	= 50 %
Resin solids required (%)	= 3 %
Dry furnish weight (lb)	= 6.25 × (1-wax-resin-additives)
	= 6.25 × (1-0.01-0.03-0.08) = 5.063
Total resin weight (lb)	= (5.063 lb × 3)/50 = 0.304 lb
Wax solids content (%)	= 50 %
Was solids required (%)	= 1 %
Total wax weight (lb)	= (dry furnish weight × wax required)/wax solids
	= (5.063 × 1)/50 = 0.101
Furnish moisture content (%)	= 4%
Mat furnish weight (lb)	= dry furnish weight/(1-furnish MC)
	= 5.063 lb/(1-0.04) = 5.273 lb
Furnish excess factor	= 10% per board = 1.10
	(for furnish loss during blending and mat forming)

Required material weights for surface layer:

	Mat solid wt.	Mat water wt.	Mat wt.	Blend wt (Mat wt.*1.1)
Furnish (lb)	5.063	0.211	5.273	5.801
Resin (lb)	0.152	0.152	0.304	0.334
Wax (lb)	0.059	0.043	0.101	0.111
Total (lb)	5.273	0.405	5.678	6.246

www.manaraa.com

Table.A.4. Oriented strand board processing calculations for 40lb/ ft^3 target density, core layer.

Target board density (lb/ft^3)	= 40 lb/ ft^3
Nominal board volume (ft^3)	= 30 in × 30 in × 0.2 in = 180 in^3= 0.1042 ft^3
Board weight (lb)	= 40 lb/ ft^3× 0.1042 ft^3= 4.17 lb
Board additive: water(%) = EMC	= 8 %
Core resin solid content (%)	= 60 %
Resin solids required (%)	= 3 %
Dry furnish weight (lb)	= 4.17 × (1-wax-resin-additives)
	= 4.17 × (1-0.01-0.03-0.08) = 3.375 (lb)
Total resin weight (lb)	= (3.375 lb × 3)/60 = 0.169 lb
Wax solids content (%)	= 50 %
Was solids required (%)	= 1 %
Total wax weight (lb)	= (dry furnish weight × wax required)/wax solids
	= (3.375 × 1)/50 = 0.068
Furnish moisture content (%)	= 4%
Mat furnish weight (lb)	= dry furnish weight/(1-furnish MC)
	= 3.375 lb/(1-0.04) = 3.516 lb
Furnish excess factor	= 10% per board = 1.10
	(for furnish loss during blending and mat forming)

Required material weights for core layer:

	Mat solid wt.	Mat water wt.	Mat wt.	Blend wt (Mat wt.*1.1)
Furnish (lb)	3.375	0.141	3.516	3.867
Resin (lb)	0.101	0.068	0.169	0.186
Wax (lb)	0.039	0.028	0.068	0.074
Total (lb)	3.515	0.236	3.752	4.127

www.manaraa.com

Table A.5. Oriented strand board processing calculations for 41lb/ ft^3 target density, surface layer.

Target board density (lb/ ft^3)	= 41 lb/ ft^3
Nominal board volume (ft^3)	= 30 in × 30 in × 0.3 in = 270 in^3= 0.1563 ft^3
Board weight (lb)	= 40 lb/ ft^3× 0.1563 ft^3= 6.41 lb
Board additive: water(%) = EMC	= 8 %
Face resin solid content (%)	= 50 %
Resin solids required (%)	= 3 %
Dry furnish weight (lb)	= 6.41 × (1-wax-resin-additives)
	= 6.41 × (1-0.01-0.03-0.08) = 5.189
Total resin weight (lb)	= (5.063 lb × 3)/50 = 0.311 lb
Wax solids content (%)	= 50 %
Was solids required (%)	= 1 %
Total wax weight (lb)	= (dry furnish weight × wax required)/wax solids
	= (5.063 × 1)/50 = 0.104
Furnish moisture content (%)	= 4%
Mat furnish weight (lb)	= dry furnish weight/(1-furnish MC)
	= 5.063 lb/(1-0.04) = 5.405 lb
Furnish excess factor	= 10% per board = 1.10
	(for furnish loss during blending and mat forming)

Required material weights for surface layer:

	Mat solid wt.	Mat water wt.	Mat wt.	Blend wt (Mat wt.*1.1)
Furnish (lb)	5.189	0.216	5.405	5.946
Resin (lb)	0.156	0.156	0.311	0.342
Wax (lb)	0.060	0.044	0.104	0.114
Total (lb)	5.405	0.415	5.820	6.402

www.manaraa.com

Table A.6. Oriented strand board processing calculations for 41lb/ ft^3 target density, core layer.

Target board density (lb/ft^3)	= 40 lb/ft^3
Nominal board volume (ft^3)	= 30 in × 30 in × 0.2 in = 180 in^3= 0.1042 ft^3
Board weight (lb)	= 40 lb/ft^3× 0.1042 ft^3= 4.27 lb
Board additive: water(%) = EMC	= 8 %
Core resin solid content (%)	= 60 %
Resin solids required (%)	= 3 %
Dry furnish weight (lb)	= 4.27 × (1-wax-resin-additives)
	= 4.27 × (1-0.01-0.03-0.08) = 3.375 (lb)
Total resin weight (lb)	= (3.375 lb × 3)/60 = 0.169 lb
Wax solids content (%)	= 50 %
Was solids required (%)	= 1 %
Total wax weight (lb)	= (dry furnish weight × wax required)/wax solids
	= (3.375 × 1)/50 = 0.068
Furnish moisture content (%)	= 4%
Mat furnish weight (lb)	= dry furnish weight/(1-furnish MC)
	= 3.375 lb/(1-0.04) = 3.516 lb
Furnish excess factor	= 10% per board = 1.10
	(for furnish loss during blending and mat forming)

Required material weights for surface layer:

	Mat solid wt.	Mat water wt.	Mat wt.	Blend wt (Mat wt.*1.1)
Furnish (lb)	3.459	0.144	3.604	3.964
Resin (lb)	0.104	0.069	0.173	0.190
Wax (lb)	0.040	0.029	0.069	0.076
Total (lb)	3.603	0.242	3.846	4.230

www.manaraa.com

Table A.7. Oriented strand board processing calculations for 42lb/ ft^3 target density, surface layer.

Target board density (lb/ ft^3)	= 42 lb/ ft^3
Nominal board volume (ft^3)	= 30 in × 30 in × 0.3 in = 270 in^3= 0.1563 ft^3
Board weight (lb)	= 42 lb/ ft^3× 0.1563 ft3 = 6.56 lb
Board additive: water(%) = EMC	= 8 %
Face resin solid content (%)	= 50 %
Resin solids required (%)	= 3 %
Dry furnish weight (lb)	= 6.56 × (1-wax-resin-additives)
	= 6.56 × (1-0.01-0.03-0.08) = 5.316
Total resin weight (lb)	= (5.316 lb × 3)/50 = 0.319 lb
Wax solids content (%)	= 50 %
Was solids required (%)	= 1 %
Total wax weight (lb)	= (dry furnish weight × wax required)/wax solids
	= (5.316 × 1)/50 = 0.106
Furnish moisture content (%)	= 4%
Mat furnish weight (lb)	= dry furnish weight/(1-furnish MC)
	= 5.316 lb/(1-0.04) = 5.537 lb
Furnish excess factor	= 10% per board = 1.10
	(for furnish loss during blending and mat forming)

Required material weights for surface layer:

	Mat solid wt.	Mat water wt.	Mat wt.	Blend wt (Mat wt.*1.1)
Furnish (lb)	5.316	0.221	5.537	6.091
Resin (lb)	0.159	0.159	0.319	0.351
Wax (lb)	0.062	0.045	0.106	0.117
Total (lb)	5.537	0.426	5.962	6.559

www.manaraa.com

Table A.8. Oriented strand board processing calculations for 42lb/ ft^3 target density, core layer.

Target board density (lb/ft^3)	= 42 lb/ft^3
Nominal board volume (ft^3)	= 30 in × 30 in × 0.2 in = 180 in^3= 0.1042 ft^3
Board weight (lb)	= 42 lb/ft^3× 0.1042 ft^3= 4.38 lb
Board additive: water(%) = EMC	= 8 %
Core resin solid content (%)	= 60 %
Resin solids required (%)	= 3 %
Dry furnish weight (lb)	= 4.38 × (1-wax-resin-additives)
	= 4.38 × (1-0.01-0.03-0.08) = 3.544 (lb)
Total resin weight (lb)	= (3.544 lb × 3)/60 = 0.177 lb
Wax solids content (%)	= 50 %
Was solids required (%)	= 1 %
Total wax weight (lb)	= (dry furnish weight × wax required)/wax solids
	= (3.544 × 1)/50 = 0.071
Furnish moisture content (%)	= 4%
Mat furnish weight (lb)	= dry furnish weight/(1-furnish MC)
	= 3.544 lb/(1-0.04) = 3.691 lb
Furnish excess factor	= 10% per board = 1.10
	(for furnish loss during blending and mat forming)

Required material weights for core layer:

	Mat solid wt.	Mat water wt.	Mat wt.	Blend wt (Mat wt.*1.1)
Furnish (lb)	3.544	0.148	3.691	4.061
Resin (lb)	0.106	0.071	0.177	0.195
Wax (lb)	0.041	0.030	0.071	0.078
Total (lb)	3.691	0.248	3.939	4.333

www.manaraa.com

Table A.9. Oriented strand board processing calculations for 45lb/ ft^3 target density, surface layer.

Target board density (lb/ft^3)	= 45 lb/ft^3
Nominal board volume (ft^3)	= 30 in × 30 in × 0.3 in = 270 in^3= 0.1563 ft^3
Board weight (lb)	= 40 lb/ft^3 × 0.1563 ft3 = 7.03 lb
Board additive: water(%) = EMC	= 8 %
Face resin solid content (%)	= 50 %
Resin solids required (%)	= 3 %
Dry furnish weight (lb)	= 7.03 × (1-wax-resin-additives)
	= 7.03 × (1-0.01-0.03-0.08) = 5.695
Total resin weight (lb)	= (5.695 lb × 3)/50 = 0.342 lb
Wax solids content (%)	= 50 %
Was solids required (%)	= 1 %
Total wax weight (lb)	= (dry furnish weight × wax required)/wax solids
	= (5.695 × 1)/50 = 0.114
Furnish moisture content (%)	= 4%
Mat furnish weight (lb)	= dry furnish weight/(1-furnish MC)
	= 5.695 lb/(1-0.04) = 5.933 lb
Furnish excess factor	= 10% per board = 1.10
	(for furnish loss during blending and mat forming)

Required material weights for surface layer:

	Mat solid wt.	Mat water wt.	Mat wt.	Blend wt (Mat wt.*1.1)
Furnish (lb)	5.695	0.237	5.933	6.526
Resin (lb)	0.171	0.171	0.342	0.376
Wax (lb)	0.066	0.048	0.114	0.125
Total (lb)	5.932	0.456	6.388	7.027

www.manaraa.com

Table A.10. Oriented strand board processing calculations for 45lb/ft^3 target density, core layer.

Target board density (lb/ft^3)	= 45 lb/ft^3
Nominal board volume (ft^3)	= 30 in × 30 in × 0.2 in = 180 in^3= 0.1042 ft^3
Board weight (lb)	= 45 lb/ft^3× 0.1042 ft^3= 4.69 lb
Board additive: water(%) = EMC	= 8 %
Core resin solid content (%)	= 60 %
Resin solids required (%)	= 3 %
Dry furnish weight (lb)	= 4.69 × (1-wax-resin-additives)
	= 4.69 × (1-0.01-0.03-0.08) = 3.797 (lb)
Total resin weight (lb)	= (3.797 lb × 3)/60 =0.190 lb
Wax solids content (%)	= 50 %
Was solids required (%)	= 1 %
Total wax weight (lb)	= (dry furnish weight × wax required)/wax solids
	= (3.797 × 1)/50 = 0.076
Furnish moisture content (%)	= 4%
Mat furnish weight (lb)	= dry furnish weight/(1-furnish MC)
	= 3.797 lb/(1-0.04) = 3.9553.516 lb
Furnish excess factor	= 10% per board = 1.10
	(for furnish loss during blending and mat forming)

Required material weights for core layer:

	Mat solid wt.	Mat water wt.	Mat wt.	Blend wt (Mat wt.*1.1)
Furnish (lb)	3.797	0.158	3.955	4.351
Resin (lb)	0.114	0.076	0.190	0.209
Wax (lb)	0.044	0.032	0.076	0.084
Total (lb)	3.955	0.266	4.221	4.643

www.manaraa.com

Table A.11. Oriented strand board processing calculations for 50lb/ft^3 target density, surface layer.

Target board density (lb/ft^3)	= 50 lb/ft^3
Nominal board volume (ft^3)	= 30 in × 30 in × 0.3 in = 270 in^3= 0.1563 ft^3
Board weight (lb)	= 50 lb/ft^3× 0.1563 ft^3= 7.81 lb
Board additive: water(%) = EMC	= 8 %
Face resin solid content (%)	= 50 %
Resin solids required (%)	= 3 %
Dry furnish weight (lb)	= 7.81 × (1-wax-resin-additives)
	= 7.81 × (1-0.01-0.03-0.08) = 6.328
Total resin weight (lb)	= (5.695 lb × 3)/50 = 0.342 lb
Wax solids content (%)	= 50 %
Was solids required (%)	= 1 %
Total wax weight (lb)	= (dry furnish weight × wax required)/wax solids
	= (6.328 × 1)/50 = 0.114
Furnish moisture content (%)	= 4%
Mat furnish weight (lb)	= dry furnish weight/(1-furnish MC)
	= 6.328 lb/(1-0.04) = 5.933 lb
Furnish excess factor	= 10% per board = 1.10
	(for furnish loss during blending and mat forming)

Required material weights for surface layer:

	Mat solid wt.	Mat water wt.	Mat wt.	Blend wt (Mat wt.*1.1)
Furnish (lb)	6.328	0.237	5.933	6.526
Resin (lb)	0.171	0.171	0.342	0.376
Wax (lb)	0.066	0.048	0.114	0.125
Total (lb)	5.932	0.456	6.388	7.027

www.manaraa.com

Table A.12. Oriented strand board processing calculations for 50lb/ft3 target density, core layer.

Target board density (lb/ft^3)	= 50 lb/ft^3
Nominal board volume (ft^3)	= 30 in × 30 in × 0.2 in = 180 in^3= 0.1042 ft^3
Board weight (lb)	= 50 lb/ft^3× 0.1042 ft^3= 5.21 lb
Board additive: water(%) = EMC	= 8 %
Core resin solid content (%)	= 60 %
Resin solids required (%)	= 3 %
Dry furnish weight (lb)	= 5.21 × (1-wax-resin-additives)
	= 5.21 × (1-0.01-0.03-0.08) = 4.219 (lb)
Total resin weight (lb)	= (4.219 lb × 3)/60 =0.211 lb
Wax solids content (%)	= 50 %
Was solids required (%)	= 1 %
Total wax weight (lb)	= (dry furnish weight × wax required)/wax solids
	= (4.219 × 1)/50 = 0.076
Furnish moisture content (%)	= 4%
Mat furnish weight (lb)	= dry furnish weight/(1-furnish MC)
	= 4.219 lb/(1-0.04) = 3.9553.516 lb
Furnish excess factor	= 10% per board = 1.10
	(for furnish loss during blending and mat forming)

Required material weights for core layer:

	Mat solid wt.	Mat water wt.	Mat wt.	Blend wt (Mat wt.*1.1)
Furnish (lb)	4.219	0.176	4.395	4.834
Resin (lb)	0.127	0.084	0.211	0.232
Wax (lb)	0.049	0.035	0.084	0.093
Total (lb)	4.394	0.296	4.690	5.159

www.manaraa.com

APPENDIX B

NORMALITY TESTS RESULTS FOR VOLTAGE ATTENUATION AND PHASE SHIFT WITH SAS UNIVARIATE PROCEDURE.

www.manaraa.com

B.1.1 Results of Normality tests for Att and Phase with SAS UNIVARIATE procedure. Relative humidity conditioning method model-building data set:

Variable: att

Basic Statistical Measures

Location		Variability	
Mean	20.76619	Std Deviation	0.72266
Median	20.92500	Variance	0.52224
Mode	19.83000	Range	2.51000
		Interquartile Range	1.28000

NOTE: The mode displayed is the smallest of 4 modes with a count of 2.

Tests for Normality

Test		--Statistic---		-----p Value------	
Shapiro-Wilk	W	0.948757	Pr < W		0.0583
Kolmogorov-Smirnov	D	0.130407	Pr > D		0.0724
Cramer-von Mises	W-Sq	0.1305	Pr > W-Sq		0.0431
Anderson-Darling	A-Sq	0.744966	Pr > A-Sq		0.0485

Normal Probability Plot

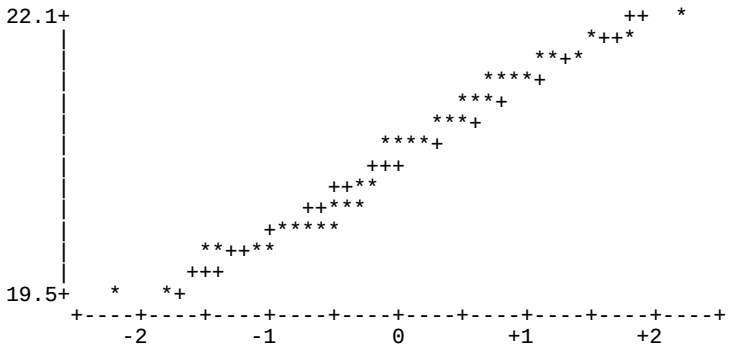

www.manaraa.com

Variable: phase

Basic Statistical Measures

Location		Variability	
Mean	-0.59476	Std Deviation	0.57623
Median	-0.50000	Variance	0.33204
Mode	-0.20000	Range	1.95000
		Interquartile Range	0.90000

Tests for Normality

Test	--Statistic---		-----p Value------	
Shapiro-Wilk	W	0.913889	Pr < W	0.0609
Kolmogorov-Smirnov	D	0.158116	Pr > D	<0.0100
Cramer-von Mises	W-Sq	0.174031	Pr > W-Sq	0.0109
Anderson-Darling	A-Sq	1.137817	Pr > A-Sq	<0.0050

Variable: phase

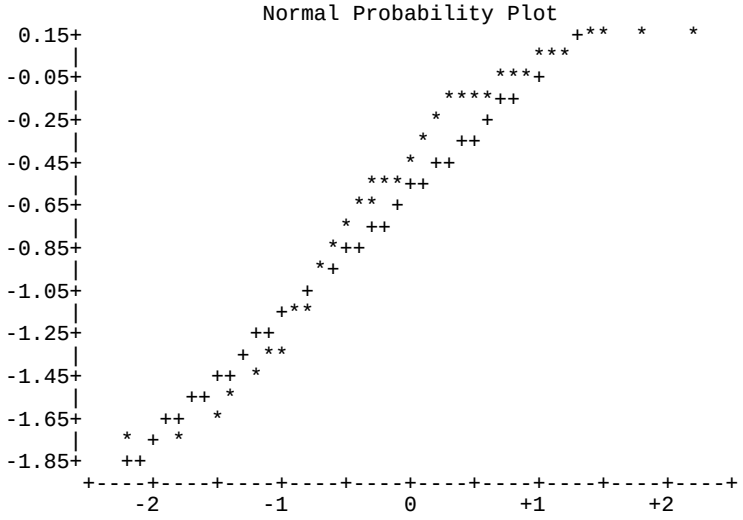

www.manaraa.com

B.1.2 Results of normality tests for Att and Phase with SAS UNIVARIATE procedure. Relative humidity conditioning method validation data set:

Variable: att

Basic Statistical Measures

Location		Variability	
Mean	20.55262	Std Deviation	0.70125
Median	20.58000	Variance	0.49175
Mode	20.25000	Range	2.78000
		Interquartile Range	1.11000

NOTE: The mode displayed is the smallest of 2 modes with a count of 2.

Tests for Normality

Test	--Statistic---		-----p Value------	
Shapiro-Wilk	W	0.979585	Pr < W	0.6455
Kolmogorov-Smirnov	D	0.095535	Pr > D	>0.1500
Cramer-von Mises	W-Sq	0.05177	Pr > W-Sq	>0.2500
Anderson-Darling	A-Sq	0.291084	Pr > A-Sq	>0.2500

Normal Probability Plot

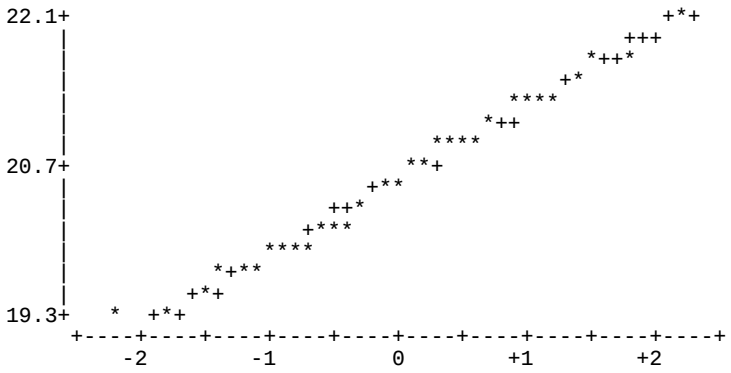

www.manaraa.com

Variable: phase

Basic Statistical Measures

Location		Variability	
Mean	-0.52071	Std Deviation	0.58579
Median	-0.40000	Variance	0.34315
Mode	-0.40000	Range	2.08000
		Interquartile Range	0.80000

NOTE: The mode displayed is the smallest of 2 modes with a count of 5.

Tests for Normality

Test		--Statistic---	-----p Value------	
Shapiro-Wilk	W	0.921371	Pr < W	0.0667
Kolmogorov-Smirnov	D	0.17687	Pr > D	<0.0100
Cramer-von Mises	W-Sq	0.167266	Pr > W-Sq	0.0144
Anderson-Darling	A-Sq	1.066971	Pr > A-Sq	0.0079

Normal Probability Plot

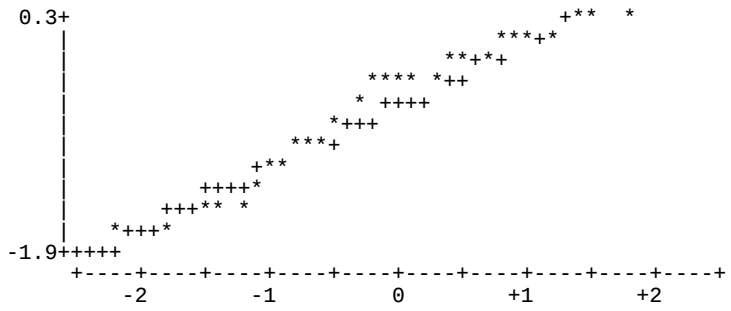

www.manaraa.com

B.2.1 Results of Normality tests for SG, MC, Attenuation and Phase shift with SAS UNIVARIATE procedure. Oven-drying conditioning method: model building data set:

Variable: att

Basic Statistical Measures

Location		Variability	
Mean	19.80877	Std Deviation	1.12935
Median	20.07000	Variance	1.27543
Mode	19.85000	Range	4.37000
		Interquartile Range	1.31000

Tests for Normality

Test	--Statistic---		-----p Value------	
Shapiro-Wilk	W	0.906167	Pr < W	<0.0621
Kolmogorov-Smirnov	D	0.129315	Pr > D	<0.0100
Cramer-von Mises	W-Sq	0.580006	Pr > W-Sq	<0.0050
Anderson-Darling	A-Sq	3.704977	Pr > A-Sq	<0.0050

Normal Probability Plot

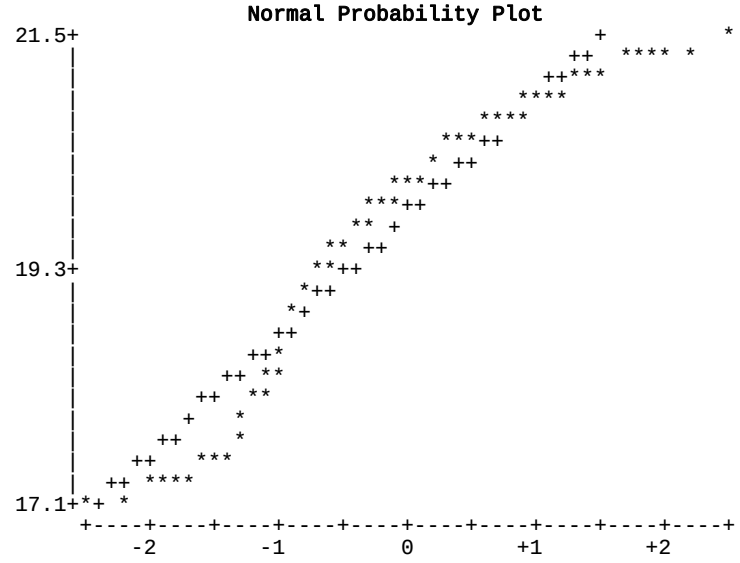

www.manaraa.com

Variable: phase

Basic Statistical Measures

Location		Variability	
Mean	-0.78705	Std Deviation	1.23443
Median	-0.50000	Variance	1.52381
Mode	-0.10000	Range	5.90000
		Interquartile Range	1.20000

Tests for Normality

Test	--Statistic---		-----p Value------	
Shapiro-Wilk	W	0.929521	Pr < W	<0.0511
Kolmogorov-Smirnov	D	0.132923	Pr > D	<0.0100
Cramer-von Mises	W-Sq	0.455197	Pr > W-Sq	<0.0050
Anderson-Darling	A-Sq	2.822793	Pr > A-Sq	<0.0050

Variable: phase

Normal Probability Plot

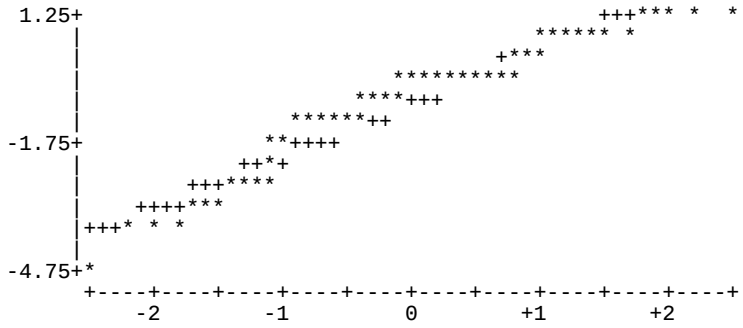

www.manaraa.com

B.2.2 Results of normality tests for SG, MC, Attenuation and Phase shift with SAS UNIVARIATE procedure. Oven-drying conditioning method: validation data set:

Variable: att
Basic Statistical Measures

Location		Variability	
Mean	19.68484	Std Deviation	1.09410
Median	19.92500	Variance	1.19705
Mode	20.51000	Range	4.72000
		Interquartile Range	1.31000

Tests for Normality

Test	--Statistic---		-----p Value------	
Shapiro-Wilk	W	0.918677	Pr < W	<0.0641
Kolmogorov-Smirnov	D	0.121141	Pr > D	<0.0100
Cramer-von Mises	W-Sq	0.526549	Pr > W-Sq	<0.0050
Anderson-Darling	A-Sq	3.218524	Pr > A-Sq	<0.0050

Normal Probability Plot

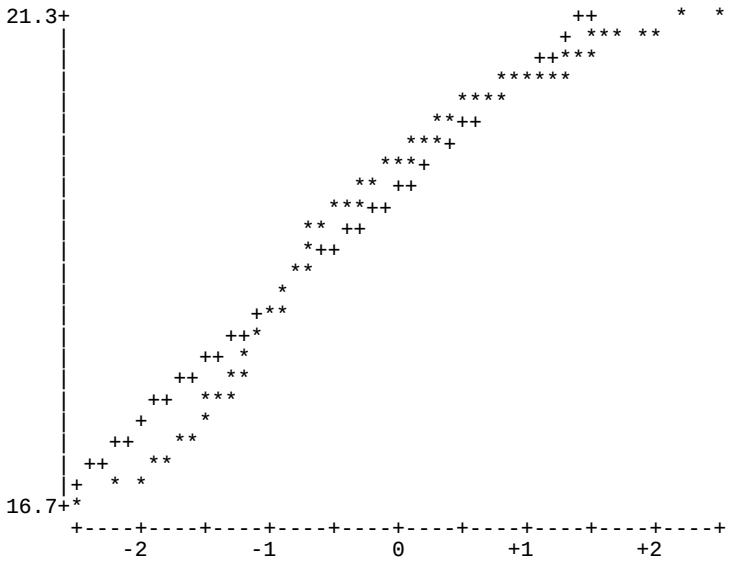

www.manaraa.com

Variable: phase

Basic Statistical Measures

Location		Variability	
Mean	-0.73952	Std Deviation	1.36821
Median	-0.50000	Variance	1.87200
Mode	-0.20000	Range	6.90000
		Interquartile Range	1.20000

Tests for Normality

Test	--Statistic---		-----p Value------	
Shapiro-Wilk	W	0.934224	Pr < W	<0.0510
Kolmogorov-Smirnov	D	0.131355	Pr > D	<0.0100
Cramer-von Mises	W-Sq	0.467644	Pr > W-Sq	<0.0050
Anderson-Darling	A-Sq	2.840465	Pr > A-Sq	<0.0050

Normal Probability Plot

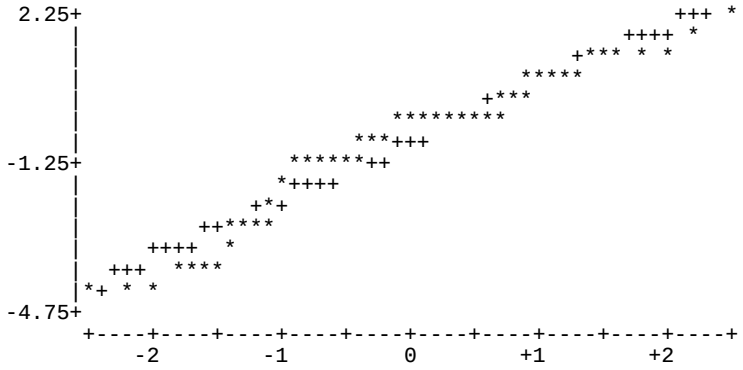

www.manaraa.com